Revision 2

Contrasting alteration textures and geochemistry of allanite from uranium-fertile and barren granites: Insights into granite-related U and ion-adsorption REE mineralization

Long Zhang[1,2,]*, Fangyue Wang[1,2,]*, Taofa Zhou[1,2], Zhenyu Chen[3]

[1]Ore Deposit and Exploration Centre, School of Resources and Environmental Engineering, Hefei University of Technology, Hefei 230009, China

[2]Anhui Province Engineering Research Center for Mineral Resources and Mine Environments, Hefei 230009, China

[3]MNR Key Laboratory of Metallogeny and Mineral Assessment, Institute of Mineral Resources, Chinese Academy of Geological Sciences, Beijing 100037, China

*Present address: No. 193, Tunxi Road, Baohe District, Hefei 230009, Anhui Province, China.

E-mail addresses: huiwonanlin@163.com (L. Zhang), fywang@hfut.edu.cn (F. Wang)

DOI: https://doi.org/10.2138/am-2022-8531. http://www.minsocam.org/

Abstract

Allanite is an important rare earth element (REE)-U-bearing mineral in granites, and it can act as a metal source for the formation of some hydrothermal uranium deposits and ion-adsorption REE deposits. To investigate the potential of allanite as a mineral probe of granite-related uranium mineralization processes and the formation of ion-adsorption REE deposits, we present textures, geochemistry, and in situ U-Pb isotope data for allanite from the fertile Changjiang granite associated with the Changjiang uranium ore field and barren Jiufeng granite in the Zhuguangshan batholith, South China. Alteration of allanite in the Changjiang granite is characterized by the altered domains with lower backscattered electron (BSE) intensities than the unaltered domains and replacement by other secondary minerals such as REE-fluorocarbonates, calcite, fluorite, thorite, clay minerals, quartz, chlorite, and epidote. Crystals from the Jiufeng granite were partly replaced by the altered domains appearing darker in BSE images and minor REE-fluorocarbonates. The darker domains of the Changjiang and Jiufeng allanite grains have higher $Fe^{3+}/(Fe^{3+} + Fe^{2+})$ ratios and U concentrations than those of the brighter domains, indicating that the alteration of allanite was probably related to more oxidized fluids. This study suggests that the Changjiang granite might have been subjected to the influx of F- and CO_2-bearing fluids.

The brighter domains of the Changjiang and Jiufeng allanite grains have weighted mean ^{207}Pb-corrected $^{206}Pb/^{238}U$ ages of 156.7 ± 4.3 Ma and 161.6 ± 5.3 Ma, respectively, consistent with the corresponding zircon $^{206}Pb/^{238}U$ ages of 156.1 ± 1.4

Ma and 159.8 ± 1.8 Ma. The darker domains of the Changjiang allanite grains yield a weighted mean $^{206}Pb/^{238}U$ age of 141.4 ± 5.6 Ma, which overlaps within error the timing of a uranium mineralization event (~140 Ma) in the Changjiang uranium ore field and the age of a crustal extension event (140−135 Ma) in South China. The BSE images and elemental maps reveal that rare earth elements such as La and Ce have been released from the Changjiang allanites during alteration and were precipitated as REE-fluorocarbonates that are susceptible to chemical weathering, which sets the stage for the formation of an ion-adsorption REE deposit. Our study suggests that the regional crustal extension might have played an important role in the formation of both granite-related uranium and ion-adsorption REE deposits in South China, as it could have triggered alteration or breakdown of REE-U-bearing minerals in source rocks.

Keywords: Allanite, mineral chemistry, geochronology, granite-related U deposits, ion-adsorption REE deposits, South China

1. INTRODUCTION

Allanite, an epidote-group mineral, has the formula as $A_2M_3Si_3O_{11}(O, F)(OH)$, where A = Ca^{2+}, Pb^{2+}, Mn^{2+}, Th^{4+}, REE^{3+}, and U^{4+}, and M = Al^{3+}, Fe^{3+}, Fe^{2+}, Mn^{2+}, Mg^{2+}, Cr^{3+}, and V^{3+} (Deer et al. 1986). Allanite has been shown to be susceptible to alteration (Wood and Ricketts 2000; Poitrasson 2002). The alteration mechanisms of allanite mainly involve the transformation of allanite to epidote and replacement by secondary allanite, REE-fluorocarbonates, calcite, fluorite, thorite, and clay minerals

(Morin 1977; Petrík et al. 1995; Wood and Ricketts 2000; Poitrasson 2002; Berger et al. 2008; Pal et al. 2011; Uher et al. 2015). Allanite has been used to study U-Th-Pb geochronology (Darling et al. 2012; Smye et al. 2014; McFarlane 2016; Liao et al. 2020), nature of associated hydrothermal fluids (Wood and Ricketts 2000; Uher et al. 2015), REE exchanges during fluid-mineral interactions (Poitrasson 2002; Pal et al. 2011), and mineralization processes (Pal et al. 2011; Chen and Zhou 2014; Deng et al. 2014; Ngo et al. 2020). Allanite is a common accessory mineral in many metaluminous and weakly peraluminous felsic rocks and is regarded to represent an important source of uranium for hydrothermal uranium deposits (Cuney 2009, 2014). Examples of this include volcanogenic uranium deposits in the Streltsovka, Russia (Chabiron et al. 2003) and sandstone-hosted uranium deposits in the Erlian Basin, China (Bonnetti et al. 2017). In some cases, secondary allanite derived from primary allanite may effectively record regional mineralization/hydrothermal events, which helps understand ore genesis (Pal et al. 2011; Chen and Zhou 2014). Therefore, allanite may be a useful tool in deciphering the sources of uranium for granite-related uranium mineralization and the timing of related hydrothermal events.

Granite-related uranium deposits are one of the most important types of uranium deposits in South China (Zhang et al. 2021a). Granite-related uranium deposits in South China are mainly hosted by Triassic (240–225 Ma) and Jurassic (170–150 Ma) granites (Zhang et al. 2017a; Zhong et al. 2019; Chi et al. 2020). Mineral explorations and scientific studies have revealed that such deposits are spatially and genetically associated with a few granitic bodies, which are regarded as uranium-fertile granites

(Zhao et al. 2011, 2016; Zhang et al. 2018a). Generally, the formation of these uranium deposits has been linked to the regional Cretaceous to Tertiary crustal extension and related mafic magmatism, which could have provided thermal energy for fluid circulation that resulted in the mobilization of uranium from U-rich rocks (Min et al. 1999; Hu et al. 2008; Mao et al. 2013; Chi et al. 2020). Previous studies have showed that the mineralization ages of granite-related uranium deposits in South China are generally consistent with the timing of regional crustal extension events (e.g., Hu et al. 2008; Luo et al. 2015; Zhong et al. 2019). However, the temporal link between uranium release from U-rich rocks and regional crustal extension events is not well constrained.

Ion-adsorption REE deposits represent the world's most important source of HREE and mainly occur in South China (Kynicky et al. 2012; Li et al. 2017; Borst et al. 2020). They generally formed from weathering of granites that contain significant proportion of accessory REE minerals susceptible to chemical weathering, such as REE-fluorocarbonates (bastnäsite, parisite, and synchysite) and phosphates (monazite, apatite, and xenotime) (Ishihara et al. 2008; Kynicky et al. 2012; Bern et al. 2017; Li et al. 2017, 2019). Alteration can transform primary REE-bearing minerals into the forms that are easier to be weathered, which is important for the formation of ion-adsorption REE deposits (Ishihara et al. 2008; Imai et al. 2012; Bern et al. 2017). Although many studies of alteration of primary REE-bearing minerals in parental rocks have discussed the mobilization of REE (e.g., Imai et al. 2012; Bern et al. 2017; Li et al. 2019; Huang et al. 2021; Zhao et al. 2022), few studies provide direct evidence for REE leaching from these minerals (Ishihara et al. 2008). Allanite is an important primary REE-bearing accessory minerals in granites related to many ion-adsorption REE deposits such as the Dingnan, Guposhan, Xiache, Zhaibei, Renju, and Huashan in South China (Li et al. 2019; Huang et al. 2021; Zhao et al. 2022). Therefore, understanding the textural and compositional evolution of allanite during alteration may also provide insights into the formation of ion-adsorption REE deposits.

Both the granite-related uranium and ion-adsorption REE deposits are typically epigenetic; their formation usually requires the remobilization of U or REE from primary U- and/or REE-bearing minerals (Ruzicka 1993; Hu et al. 2008; Ishihara et al. 2008; Cuney 2014; Li et al. 2019). Thus, understanding the alteration of allanite-bearing granites may be important to deciphering the genesis of granite-related U and ion-adsorption REE mineralization. The Zhuguangshan batholith is one of the most important granite-related uranium ore producers in South China; it hosts the Changjiang, Lanhe, Baishun, and Chengkou uranium ore fields (Zhang et al. 2017a; Zhong et al. 2019). The Changjiang uranium ore field, which contains >10,000 tonnes of recoverable uranium with a grade of 0.1–0.5%, is one of the most important uranium ore fields in South China (Zhang et al. 2017a). Furthermore, two ion-adsorption REE deposits have been found in this batholith (Li et al. 2017). In this batholith, uranium deposits are associated with several plutons such as the Changjiang, Youdong, Longhuashan, and Baiyun granites, but economic uranium mineralization has not been found in the Jiufeng and Fuxi granites (Zhang et al. 2018a). Allanite, an important REE-bearing accessory mineral in both the uranium-fertile Changjiang and barren Jiufeng granites, shows complex alteration textures. Here, we present textures, geochemistry, and in situ U-Pb geochronologic data for allanite from these two granites, with the aim to investigate the temporal link between uranium release from U-rich rocks and the regional crustal extension and direct evidence for REE leaching from primary REE-bearing minerals. This study provides new insights into granite-related uranium mineralization processes and the formation of ion-adsorption REE deposits in South China.

2. GEOLOGICAL SETTING

2.1. Regional Geology

South China contains the largest number of known uranium deposits and the largest uranium resources in China (Dahlkamp 2009; Zhang et al. 2020a). Granite-related uranium deposits in this region are mainly distributed in the Cathaysia Block and the Jiangnan Orogen (Fig. 1) and represent one of the most important types of uranium deposits in China. They are mainly hosted by or occur adjacent to granites and formed at around 110–50 Ma (Hu et al. 2008; Bonnetti et al. 2018; Zhong et al. 2019; Chi et al. 2020). Most of the granites related to uranium mineralization are of Triassic (251–205 Ma) and Jurassic age (180–142 Ma; Zhao et al. 2011, 2016; Chen et al. 2012; Zhang et al. 2017b, 2018a; Chi et al. 2020). The formation of granite-related uranium deposits in this region has been linked to regional crustal extension events (Hu et al. 2008; Luo et al. 2015; Zhong et al. 2019; Chi et al. 2020). South China was in an extensional tectonic regime during the Cretaceous to Tertiary

DOI: https://doi.org/10.2138/am-2022-8531. http://www.minsocam.org/

with six major episodes of extension taking place at 140−135 Ma, 125−120, 110−100 Ma, 95−85 Ma, 75−70 Ma, and 55−45 Ma (Li and McCulloch 1998; Li 2000; Hu et al. 2004, 2008). The mineralizing system of granite-related uranium deposits in South China generally consists of leaching of uranium from U-rich granites triggered by the regional Cretaceous to Tertiary crustal extension and related mafic magmatism, transport of uranium as uranyl-carbonate, uranyl-fluorine-carbonate, and uranyl-chloride complexes in hydrothermal fluids, and deposition of uranium associated with a decrease of oxygen fugacity (Hu et al. 2008; Zhang et al. 2017a; Chi et al. 2020).

The Zhuguangshan batholith is mainly composed of Silurian (420−435 Ma), Triassic (225−240 Ma) and Jurassic (150−165 Ma) biotite granite and two-mica granite, with minor Cretaceous granites (Fig. 2; Deng et al. 2012; Zhang et al. 2017b, 2018a; Chi et al. 2020). Uranium deposits in this area are associated with several plutons such as the Changjiang, Youdong, Longhuashan, and Baiyun granites (Zhang et al. 2018a). The uranium mineralizing events in the Zhuguangshan area mainly took place in five episodes, ~140 Ma, ~125 Ma, ~105 Ma, ~90 Ma, and 80−60 Ma (Zhang et al. 2017b; Bonnetti et al. 2018; Zhong et al. 2019). Mafic dykes intruding the Zhuguangshan batholith are oriented in WNW, ENE, and NNE directions with WNW-trending dykes being dominantly distributed in the eastern part the batholith (Fig. 2). These mafic dykes were mainly emplaced in three episodes, ~140 Ma, ~105 Ma, and ~90 Ma (Li and McCulloch 1998; Zhang et al. 2018a).

South China is also known for its endowment of ion-adsorption REE deposits, which are mainly distributed over Jiangxi, Guangdong, Fujian, Hunan, Guangxi and Yunnan provinces (Fig. 1, Xie et al. 2016; Li et al. 2017). These deposits generally can be classified as the LREE-dominated and HREE-dominated types, and the majority of them originated from granites and volcanic tuff with ages ranging from the Ordovician to the late Cretaceous (Li et al. 2017). There are many ion-adsorption REE deposits such as the Zudong, Pitou, and Zhaibei adjacent to the Zhuguangshan batholith, and two ion-adsorption REE deposits have been found in this batholith (Fig. 1). The regolith profiles of ion-adsorption REE deposits in South China generally include a humic layer, completely weathered zone, semi-weathered zone, and unweathered bedrock (Wu et al. 1990; Li et al. 2017; Fu et al. 2019). Orebodies (REE-enriched soil horizons) are usually located at the lower completely-weathered zone and upper semi-weathered zone; the content of clay minerals in orebodies can reach up to 80% (Wu et al. 1990; Li et al. 2017).

2.2. Geology of the Changjiang uranium ore field

The Changjiang uranium ore field is located in the southeastern part of the Zhuguangshan granitic batholith. There are several economic uranium deposits such as the 301, 302, 305, and 306; the 302 deposit is the largest granite-hosted uranium deposit in South China (Zhong et al. 2019). Uranium deposits in this area are mainly hosted by the Changjiang and Youdong granites. Zircon U-Pb dating indicates that the Changjiang and Youdong granites have emplacement ages of 157.6 ± 1.8 Ma and 226.4 ± 3.5 Ma, respectively (Zhang et al. 2017b, 2018a). The Youdong two-mica granite has a major mineral assemblage of quartz, K-feldspar, plagioclase, biotite, and muscovite (Zhang et al. 2021b). The Changjiang pluton consists of biotite granite and has a major mineral assemblage of quartz, K-feldspar, plagioclase, and biotite (Zhang et al. 2021b). In the Changjiang and Youdong granites, biotite was partly or completely replaced by chlorite, and feldspars were partly replaced by illite (Zhang et al. 2021b).

Several mafic dikes intruded the Changjiang uranium ore deposit and there are several NE–SW striking regional faults such as the Mianhuakeng, Lizhou, and Huangxishui, and NW–SE striking faults such as the Youdong (Zhong et al. 2019). The uranium mineralization occurs both in veins and alteration halos in, or close to, fracture zones within granites. The veins usually consist of quartz, fluorite, calcite, hematite, pitchblende (fine-grained aggregates of uraninite), and pyrite. Pitchblende is the main uranium ore mineral in the Changjiang uranium ore field. Pitchblende U-Pb dating indicates that the uranium mineralization in this area mainly took place in five episodes, ~140 Ma, ~125 Ma, ~105 Ma, ~90 Ma, and 80–60 Ma (Zhang et al. 2017b; Bonnetti et al. 2018; Zhong et al. 2019).

3. Samples and analytical methods

3.1. Samples and descriptions

A total of thirty-two samples were collected from outcrops and drill cores from the Changjiang and Jiufeng granites. Twenty-five samples collected from drill hole KZK11-3 in the 302 uranium deposit within the Changjiang granite were taken. Uranium mineralization mainly occurs between 156 to 159 m. Fifteen samples were collected at approximately one-meter intervals from 141 to 156 m, and ten samples were collected from 157 to 174 m. The detailed description of the drill hole can also be seen the study of Zhang et al. (2018b) in which a schematic profile of the drill hole was provided. The investigated samples are the mineralized rocks and the altered granites close to uranium mineralization. U-bearing accessory minerals of the Changjiang granite include zircon, apatite, uraninite, monazite, allanite, uranothorite, and xenotime (Figs. 3a-3c). Seven samples were collected from outcrops of the Jiufeng granite; the alteration minerals are chlorite and illite (Fig. 3d). It has a U-bearing accessory mineral assemblage of zircon, apatite, allanite, uranothorite, titanite, minor uraninite and monazite. Uranium mineralization in the studied samples occurs as veins that mainly consists of quartz, fluorite, pitchblende, pyrite, sericite, and calcite (Figs. 3e and 3f); the close association of these minerals probably supports co-precipitation.

3.2. SEM analyses

Back-scattered electron (BSE) images were obtained by a TESCAN MIRA3 field emission scanning election microscope equipped with energy-dispersive X-ray spectrometer (EDS) at the Ore Deposit and Exploration Centre (ODEC), Hefei University of Technology, China. The operating conditions were 15 kV accelerating voltage and 10 nA beam current (Zhang et al. 2021b).

3.3. EPMA analyses

Quantitative analyses and element mapping of allanite were performed using a JEOL JXA-8230 EPMA at the Key Laboratory of Metallogeny and Mineral

Assessment, Chinese Academy of Geological Sciences, Beijing, China. The operating conditions were 15 kV accelerating voltage and a beam current of 50 nA, with variable counting times (10 to 40 s on peaks, 5 to 20 s on background). The beam diameter ranged from 1 to 5 μm, and a ZAF matrix correction was applied during data reduction. The following standards and crystals were used for microanalyses: wollastonite (Ca-Kα, PETH), hematite (Fe-Kα, LIF), jadeite (Al-Kα, TAP; Si-Kα, PETJ), forsterite (Mg-Kα, TAP), topaz (F-Kα, TAP), UO_2 (U-Mα, PETH), ThO_2 (Th-Mα, PETH), and rutile (Ti-Kα, LIF). Synthetic rare earth pentaphosphate crystals were used as standards for REE. The operating conditions for element mapping were 15 kV accelerating voltage with 100 nA beam current, 0.5 μm step size, and 50 ms dwell time; The detailed analytical technique is similar to that described in Zhang et al. (2020b). The $Fe^{3+}/(Fe^{2+} + Fe^{3+})$ ratio for allanite is calculated using the equation $Fe^{3+}/(Fe^{2+} + Fe^{3+}) = (REE^{3+} + Th^{4+})/(Al^{3+} - 3) + 1$ on the basis of atoms per formula unit (Poitrasson 2002).

3.4. LA-ICP-MS analyses

In situ allanite and zircon U-Th-Pb isotopes and trace element analyses were conducted by LA-ICP-MS at the ODEC, Hefei University of Technology, using an Agilent 7900 ICP-MS Coupled to a Teledyne Cetac Technologies Analyte Excite laser ablation system with a 193 nm ArF excimer laser. Analyses were carried out with a laser beam diameter of 30 μm and repetition rate of 7 Hz, and each spot analysis incorporated a background acquisition of approximately 20 s, followed by 40 s sample data acquisition. The standard zircon GEMOC GJ-1 (Jackson et al. 2004) was used to correct for the mass discrimination of the mass spectrometer and any elemental fractionation, and the standard zircon 91500 (Wiedenbeck et al. 1995) was used as an internal standard to assess the reproducibility and instrument stability. Trace element contents were calibrated using Si drawn from average SiO_2 values determined by EPMA as the internal standard with NIST 610 as the external standard. The analytical uncertainties were <10% for most of trace element analyses. The detailed analytical technique is similar to that described in Wang et al. (2017).

4. RESULTS

4.1. Textures of allanite

Allanite occurs as euhedral or subhedral crystals in the Changjiang and Jiufeng granites. The size of allanite gains can be up to 2 mm as observed in thin sections. Some allanite crystals are variably affected by post-magmatic transformations. Detailed petrographic observations indicate that some allanite grains show textural heterogeneity (Fig. 4). The BSE images show that allanite crystals from these two granites can be divided into two types of domains, which are characterized by different levels of grey: the brighter domains and darker domains (Fig. 4). These two types of domains are separated by a sharp boundary on BSE images. The brighter domains have a homogeneous level of grey, concentrated in grain cores and along margins.

In the Jiufeng granite, alteration of allanite is indicated by the altered domains appearing darker in BSE images than the unaltered domains with minor REE-fluorocarbonates (Figs. 4g-4l). In contrast, allanites in the Changjiang granite

DOI: https://doi.org/10.2138/am-2022-8531. http://www.minsocam.org/

show complex alteration features (Figs. 4a-4f and 5). In this pluton, inclusions of apatite and zircon are sometimes present within allanite grains (Figs. 4a-4d). Furthermore, alteration of allanite is characterized by the altered domains with lower BSE intensities than the unaltered domains (Figs. 4b-4f) and the replacement by other minerals such as REE-fluorocarbonates, calcite, fluorite, thorite, clay minerals, chlorite, quartz, and epidote (Fig. 5). These alteration features have also been observed in other studies (Petrík et al. 1995; Poitrasson 2002; Pal et al. 2011; Walters et al. 2013; Chen and Zhou 2014). There are numerous micro-cracks inside the allanite grains, and REE-fluorocarbonates fill these sites (Figs. 5a-5h). Some microveinlets of REE-fluorocarbonates are also present along the grain boundaries or micro-cracks within rock-forming minerals such as feldspars and quartz (Fig. 4c). REE-fluorocarbonates are shown as differing grey levels under BSE imaging (Fig. 5c), indicating the variable average atomic number.

4.2. Compositions of allanite

The EPMA elemental data of allanite from the Changjiang and Jiufeng granites are provided in Supplementary Table S1. In the Changjiang granite, the darker domains have lower concentrations of FeO (6.94–13.41 wt%), La_2O_3 (1.39–2.39 wt%), and Pr_2O_3 (1.74–2.40 wt%) and higher concentrations of ThO_2 (0.97–2.10 wt%) and F (0.13–0.81 wt%) than the brighter domains. Element mapping (Figs. 6 and 7) showing the compositional changes of allanite during alteration demonstrates that rare earth elements such as La and Ce were mobilized from allanite and precipitated as REE-fluorocarbonates. In the Jiufeng granite, the darker domains of allanite grains have lower contents of Fe, Al, Ca, and ΣREE, but higher contents of Th and Pb than those of the brighter domains (Fig. 8).

The diagram of ΣREE against Al (Fig. 9, after Petrík et al. 1995) and EPMA data indicate that although both the brighter and darker domains of allanites from the Changjiang granite are close to the allanite-ferriallanite end member, the darker domains have slightly higher average $Fe^{3+}/(Fe^{3+} + Fe^{2+})$ ratios (mean = 0.36) than those of the brighter domains (mean = 0.33). The analyses of darker domains of the Jiufeng allanites plot below the line of ferriallanite-epidote, and their $Fe^{3+}/(Fe^{3+} + Fe^{2+})$ ratios (mean = 0.69) are much higher than those of the unaltered domains (mean = 0.35).

The LA-ICP-MS trace element data of allanites from the Changjiang and Jiufeng granites are provided in Supplementary Table S2. Compared to the brighter domains, the darker domains of allanite grains from both the Changjiang and Jiufeng granites have elevated concentrations of U and Th. The REE patterns in all the investigated allanites are strongly LREE-enriched with negative Eu anomalies (Fig. 10). Brighter domains of the Changjiang allanites have higher $(Sm/Nd)_N$ ratios and stronger negative Eu anomalies than those of the Jiufeng allanites. Allanite grains from both the Changjiang and Jiufeng granites show greater extents of HREE depletion in the bright domains than those of the corresponding darker domains.

4.3. Compositions of other minerals

The EPMA data (Supplementary Table S3) show that REE-fluorocarbonates replacing allanites from the Changjiang granite are mainly composed of light REE

(La_2O_3 + Ce_2O_3 + Pr_2O_3 + Nd_2O_3 + Sm_2O_3 = 54.13−68.10 wt%), F (5.47−7.69 wt%), and variable CaO (2.89−14.50 wt%), thus the mineral may be bastnäesite or synchysite. Thorite replacing the Changjiang allanites (Figs. 5b and 5j) has ThO_2 abundances in the range of 64.01−68.88 wt%, SiO_2 between 18.00 and 20.02 wt%, and a wide range of UO_2 concentrations (1.26−6.10 wt%). Additionally, it contains minor CaO (1.37−1.85 wt%) and FeO (0.71−1.13 wt%).

The chemical composition data of chlorite that is the alteration product of the Changjiang allanites (Fig. 5d) are provided in Supplementary Table S3. Chlorite has concentrations of FeO in the range of 30.92−31.37 wt%, SiO_2 of 25.39−25.90 wt%, Al_2O_3 of 17.32−18.71 wt%, and MgO of 7.78−9.68 wt%.

4.4. Zircon U-Pb geochronology

Zircon grains from the Changjiang and Jiufeng granites are generally euhedral and range in size from 50 to 200 μm. Most zircon crystals display oscillatory zoning in the CL images (Fig. 11), which are typical of magmatic zircons. The results of LA-ICP-MS U-Pb analyses of zircons from these two granites are provided in Supplementary Table S4 and plotted in the concordia diagrams (Fig. 11). A total of 16 analyses on 16 zircon grains separated from the Changjiang granite yield a weighted mean age of 156.1 ± 1.4 Ma (n = 16, MSWD = 0.47) (Fig. 11a). In addition, 15 spots analyzed on 15 zircon grains from the Jiufeng granite yield a weighted mean age of 159.8 ± 1.8 Ma (n = 15, MSWD = 1.5) (Fig. 11b).

4.5. Allanite U-Pb geochronology

Allanite LA-ICP-MS U-Pb isotopic data are provided in Supplementary Table S5 and graphically illustrated in Fig. 12. Data reduction and age calculation were carried out following the procedures of Gregory et al. (2007) and Darling et al. (2012). Twenty-one spot analyses were obtained from brighter domains of the Changjiang allanite grains, and the uncorrected data define a linear array with a lower intercept age of 162.4 ± 8.3 Ma (MSWD = 0.92) in the Tera-Wasserburg diagram (Fig. 12a). All ^{207}Pb-corrected ^{206}Pb/^{238}U ages have a weighted mean age of 156.7 ± 4.3 Ma (MSWD = 0.96, Fig. 12b). This age is consistent with the weighted mean ^{206}Pb/^{238}U age of 156.1 ± 1.4 Ma (Fig. 11a) for zircons from the Changjiang granite.

Twenty spot analyses were obtained from darker domains of the Changjiang allanite grains. The uncorrected data define a linear array with a lower intercept age of 143.1 ± 8.3 Ma (MSWD = 0.83) in the Tera-Wasserburg diagram (Fig. 12c), and these analyses yield a weighted mean ^{207}Pb-corrected ^{206}Pb/^{238}U age of 141.4 ± 5.6 Ma (MSWD = 1.5, Fig. 12d).

Fifteen spot analyses were obtained from brighter domains of the Jiufeng allanite grains, and the analyses define a linear array with a lower intercept age of 163.5 ± 8.4 Ma (MSWD = 0.53) in the Tera-Wasserburg diagram (Fig. 12e). They yield a weighted mean ^{207}Pb-corrected ^{206}Pb/^{238}U age of 161.6 ± 5.3 Ma (MSWD = 0.15, Fig. 12f), which overlaps the weighted mean ^{206}Pb/^{238}U age of 159.8 ± 1.8 Ma (Fig. 11b) for the Jiufeng zircons.

5. Discussion

5.1. Alteration of allanite and its constraints on the nature of fluids

Allanite of hydrothermal origin generally forms as a result of alteration of previous REE- and Th-rich minerals such as monazite and allanite (Poitrasson 2002; Smith et al. 2002; Skrzypek et al. 2020) or through precipitation from REE-rich fluids (Banks et al. 1994; Deng et al. 2014; Ngo et al. 2020). In the Changjiang granite, some allanite grains contain irregular, BSE-dark domains, whereas others were partly replaced by other secondary minerals such as REE-fluorocarbonates, calcite, fluorite, thorite, clay minerals, quartz, chlorite, and epidote (Figs. 4b-4f and 5). The darker domains have irregular boundaries and patchy levels of grey, suggesting a lowering of the mean atomic number and the secondary nature (Poitrasson 2002; Walters et al. 2013). The textural interpretation of a later hydrothermal event superimposed on the brighter domains is further substantiated by in situ U-Pb dating in this study. The cation correlation diagram (Fig. 13a) suggests that the alteration is associated with chemical exchange between the primary allanite and fluids following the substitution mechanism of $La^{3+} + Ce^{3+} + Fe^{2+} + Fe^{3+} \leftrightarrow Si^{4+} + Th^{4+} + Al^{3+}$. Elements such as La, Ce, and Ca in the A sites can be released from allanite during alteration (Figs. 6b, 6c, and 7) and then they may form REE-fluorocarbonates (Littlejohn 1981). The similarity between REE distribution patterns of the brighter domains and darker domains of the Changjiang allanite grains suggests a genetic link (Figs. 10a and 10b).

The occurrence of alteration products of allanite mainly depends on the local chemical conditions and chemical compositions of the original allanite (e.g., Littlejohn 1981; Uher et al. 2015). The formation of secondary minerals such as fluorite, calcite, and REE-fluorocarbonates (Figs. 3f and 5) indicates that the Changjiang granite might have been subjected to the influx of F- and CO_2-bearing fluids. This is also supported by the elevated F concentrations (mean = 0.15 wt%) in the secondary allanite domains compared to the primary allanite (mean = 0.08 wt%). It is likely that the alteration of allanite and the removal of REE and U were facilitated by the formation of fluoride and carbonate complexes (Langmuir 1978; Wood 1990; Migdisov et al. 2016). Therefore, REE and U could be readily released from allanite in the F- and CO_2-bearing fluids and were redeposited as REE-fluorocarbonates near or within the original allanite (Fig. 5). Although both Th and U can be mobilized in the presence of fluoride, Th solubility in hydrothermal fluids is generally several orders of magnitude lower than the U solubility (Keppler and Wyllie 1990; Bailey and Ragnarsdottir 1994). Furthermore, CO_2 can form complexes with U, but not with Th (Keppler and Wyllie 1990). These features would lead to the fractionation of Th from U and REE during alteration of allanite. Thorium therefore tends to remain as thorite within the residual allanite rather than microveinlets hosting Th (Fig. 5). The remaining components generally form amorphous aluminosilicates such as clay minerals (Figs. 5i-5l) (Littlejohn 1981).

In contrast, allanite crystals in the Jiufeng granite were partly replaced by the altered domains appearing darker in BSE images and minor REE-fluorocarbonates during alteration (Figs. 4g-4l). The compositional change of the Jiufeng allanites during alteration can be expressed by the chemical substitution of $REE^{3+} + Fe^{2+} \leftrightarrow$

Ca^{2+} + Fe^{3+} (Fig. 13b), which means that alteration transforms allanite into epidote (Gieré and Sorensen 2004). Alteration of allanite results in the deficiency of A-sites and overfilling of M-crystallographic sites (Fig. 8d). The amount of REE-fluorocarbonates replacing allanite grains from the Jiufeng granite is much lower than those of the Changjiang granite, and the other F- and CO_2-bearing secondary minerals such as fluorite and calcite are absent. This phenomenon may have resulted from the lack of available F- and CO_2-bearing fluids for the Jiufeng granite.

The formation of REE-fluorocarbonates and clay minerals at the expense of allanite is generally suggested as a relatively low-temperature process (Wood and Ricktts 2000; Middleton et al. 2013; Uher et al. 2015). For example, the replacement of allanite in the A-type granite from Stupné (Slovakia) by REE-fluorocarbonates and calcite is suggested to take place at ≤300 °C (Uher et al. 2015). In this study, formation temperatures of the chlorite were calculated based on the geothermometric expression proposed by Battaglia (1999). The formation temperatures range from 202 °C to 210 °C, which are consistent with the formation temperatures of chlorite that is the alteration product of magmatic biotite in the Changjiang granite (210−260 °C, Zhang et al. 2017b). These results suggest that the fluids responsible for alteration of the investigated allanites are characterized by relatively low temperatures. The darker domains of allanite grains from both the Changjiang and Jiufeng granites have relatively higher $Fe^{3+}/(Fe^{3+} + Fe^{2+})$ ratios than those of the corresponding brighter domains (Fig. 9), suggesting that alteration of allanite was probably related to more oxidized fluids (Pal et al. 2011; Chen and Zhou 2014). The conclusion that the fluids responsible for allanite alteration was relatively oxidized is further supported by the higher U concentrations of the darker domains compared to the brighter domains (Supplementary Table S2) (Pal et al. 2011). Generally, uranium is highly soluble in the U^{6+} state as various uranyl complexes in oxidizing solutions, and precipitates in the U^{4+} state (Romberger 1984; Cuney 2009). Zhang et al. (2021b) suggested that U in the Changjiang granite is mainly hosted by uraninite, and U was released from this mineral during alteration. The fluids therefore may have had relatively high U concentrations, which would have yielded higher U concentrations in the darker domains relative to the brighter ones. It is possible that U^{+6} in the fluids promoted the oxidation of Fe^{+2} to Fe^{+3} in allanite and was then reduced in the U^{4+} state to be incorporated into the darker domains (Pal et al. 2011).

The fluid evolution path in the Changjiang uranium ore field may be drawn based on the hydrothermal mineral assemblages (Fig. 14). In the studied samples, the alteration minerals are dominated by chlorite and illite; biotite was replaced by chlorite, and feldspars were partly replaced by illite (Figs. 3a and 3d). Allanite was partly replaced by clay minerals (probably kaolinite) (Figs. 5i-5l). As shown in Fig. 14, mineral assemblages in area II are characterized by argillic alteration (kaolinite and/or montmorillonite) accompanied by hematite and/or iron carbonate; area III plots within the sericite and chlorite stability fields (Romberger 1984). The alteration assemblage in the investigated samples indicates that the alteration might occur in the field A (Fig. 14). The conditions involving fO_2 and pH of pitchblende precipitation in granite-related uranium deposits form South China have been investigated by several studies (Hu and Jin 1990; Zhang 1990; Zhang and Zhang 1991). For example, the ore-forming fluids at the pre-ore and syn-ore stages of the Xiwang granite-related uranium deposit adjacent to the Changjiang ore field have pH values of 6.08 to 6.14 and 4.69 to 5.09, respectively (Hu and Jin 1990). Pitchblende was precipitated from hydrothermal fluids with logfO_2 of about -40.09 in the 6217 granite-related uranium deposit, South China (Zhang 1990). The logfO_2 and pH values of ore-forming fluids of uranium deposits in the Changjiang ore field could be comparable to those two uranium deposits because granite-related uranium deposits in South China generally formed under the similar geological setting (Hu et al. 2004, 2008; Chi et al. 2020). Furthermore, quartz, fluorite, uraninite, pyrite, sericite, and calcite are the typical mineral assemblage of mineralization veins in the investigated samples (Figs. 3e and 3f). Uranium deposits such as the 301, 302, and 305 in the ore field have the same mineral assemblage (Zhong et al. 2019; Zhang et al. 2020a). These results suggest that pitchblende was precipitated from ore-forming fluids with logfO_2 of about -42 to -38 and pH of about 4.5 to 5.5 of the Changjiang uranium ore field (field B in Fig. 14).

5.2. Allanite U-Pb ages and implications for uranium mineralization

The U-Pb isotope analyses of the brighter and darker domains of allanite grains yielded distinct ages (Fig. 12). The brighter domains of allanite grains, interpreted as primary, have weighted mean ages of 156.7 ± 4.3 Ma and 161.6 ± 5.3 Ma, respectively, and these ages overlap within error the corresponding zircon U-Pb ages of 156.1 ± 1.4 Ma and 159.8 ± 1.8 Ma. Both the Changjiang and Jiufeng granites belongs to a high-K calc-alkaline association with variable CaO concentrations ranging from 0.27 to 1.75 wt% and 1.41 to 2.62 wt%, respectively (Zhang et al. 2017b, 2021b), which may favor the crystallization of allanite (Cuney and Friedrich 1987; Cuney 2009). The U-Pb results corroborate textural assessment that the BSE-brighter domains of allanites are magmatic in origin.

Pal et al. (2011) reported late allanite derived from alteration of early REE-rich allanite with ages of 1665 ± 12 Ma and 1025 ± 15 Ma and suggested multiple events of hydrothermal fluid fluxes at the Bagjata uranium mine, India. Chen and Zhou (2014) suggested that two younger hydrothermal events totally reset the U-Pb systems of primary allanite grains at the Lala Fe-Cu deposit (SW China), and the secondary allanite is dated at two clusters of concordant ages as ~880 and ~850 Ma. Therefore, the secondary allanite modified from primary allanite may effectively record the related events of hydrothermal fluid flux. In the current study, the darker domains of the Changjiang allanites have a weighted mean U-Pb age of 141.4 ± 5.6 Ma (Fig. 12d), which implies that the later hydrothermal events might have totally reset the U-Pb systems of the allanites.

It has been suggested that the formation of granite-related uranium deposits in South China is linked to regional Cretaceous to Tertiary crustal extension (Hu et al. 2008; Mao et al. 2013; Luo et al. 2015; Chi et al. 2020). In the Zhuguangshan area, the uranium mineralization took place in five episodes, ~140 Ma, ~125 Ma, ~105 Ma, ~90 Ma, and 80–60 Ma (Zhang et al. 2017b; Bonnetti et al. 2018; Zhong et al. 2019), which are consistent with the emplacement ages of mafic dykes in the Zhuguangshan area (~140 Ma, ~105 Ma, and ~90 Ma, Li and McCulloch 1998) or the ages of crustal

DOI: https://doi.org/10.2138/am-2022-8531. http://www.minsocam.org/

extension events in South China (140–135 Ma, 125–120, 110–100 Ma, 95–85 Ma, 75–70 Ma, and 55–45 Ma, Li 2000; Hu et al. 2004, 2008). The samples BD-25 and BD-27 collected from two diabase dykes in the Changjiang uranium ore field have hornblende Ar-Ar ages of 140.2 ± 2.8 Ma and 142.6 ± 2.9 Ma, respectively (Li and McCulloch 1998). In addition, Zhang et al. (2018a) reported a hornblende Ar-Ar age of 145.1 ± 1.5 Ma for one diabase dyke in this area. Secondary apatite that is the alteration product of magmatic monazite and xenotime from the uranium-fertile Douzhanshan granite (South China) yielded an EPMA U-Th-Pb chemical age of 136 ± 17 Ma, which is suggested to record a crustal extension event in South China (140–135 Ma) (Hu et al. 2013). The U-Pb age of the darker domains of the Changjiang allanites is consistent with the timing of the ~140 Ma uranium mineralization event in the Changjiang uranium ore field and the emplacement ages of ~140 Ma mafic dykes, which likely suggests a causative link between them. The major uranium mineralization in this area took place during 80–60 Ma (Zhong et al. 2019), which is at least 10 Ma later than the emplacement age (~90 Ma) of youngest mafic dykes in this area. The occurrence of the major uranium mineralization is associated with the 80–60 Ma regional crustal extension and related Cretaceous-Neogene red bed basins (Hu et al. 2008; Zhang et al. 2017a; Zhong et al. 2019). Magmatism that accompanied the extensional stress regime might have triggered the alteration or breakdown of U-bearing accessory minerals in granites (Zhang et al. 2021b). Alteration can be manifested as U-rich microveinlets that permit easier mobilization of U (Figs. 7a and 7i). Furthermore, U-rich microveinlets along grain boundaries near altered uraninites were also observed in the Changjiang granite (Zhang et al. 2021b). These would set the stage for the major uranium mineralization in this area.

5.3. Implications for the formation of ion-adsorption REE deposits in South China

In South China, the majority of ion-adsorption REE deposits formed from weathering of biotite and muscovite granites, syenite, monzogranite, granodiorite, granite porphyry, and rhyolitic tuff (Wu et al. 1990; Ishihara et al. 2008; Li et al. 2017). Biotite granites related to these deposits typically contain a primary REE-bearing accessory mineral assemblage of zircon, allanite, monazite, apatite, and titanite; allanite is usually an important host of REE (Li et al. 2017; Zhao et al. 2022). Therefore, understanding textural and compositional evolution of allanite during alteration helps decode the REE mobilization and enrichment in ion-adsorption REE deposits (Ishihara et al. 2008; Bern et al. 2017).

The Changjiang pluton, a representative biotite granite in South China, has a REE-bearing accessory mineral assemblage of zircon, apatite, allanite, uraninite, thorite, monazite, and xenotime (Zhang et al. 2021b). In this study, rare earth elements such as La and Ce have been released from allanite during fluid infiltration, and were precipitated as REE-fluorocarbonates within the cracks in allanite grains and major minerals (Figs. 4c, 5, and 7a). Previous studies suggest that hydrothermal alteration play a critical role in the formation of ion-adsorption REE deposits because it can help transform REE-bearing minerals into the forms that allow REE to be more easily

This is the peer-reviewed, final accepted version for American Mineralogist, published by the Mineralogical Society of America.
The published version is subject to change. Cite as Authors (Year) Title. American Mineralogist, in press.
DOI: https://doi.org/10.2138/am-2022-8531. http://www.minsocam.org/

extracted (Imai et al. 2012; Bern et al. 2017; Zhao et al. 2022). Our in situ U-Pb dating indicates that the darker domains of the Changjiang allanite grains yielded a weighted mean age of 141.4 ± 5.6 Ma, consistent with the timing of a crustal extension event (140−135 Ma) in South China. Therefore, the regional crustal extension might have played an important role in the formation of ion-adsorption REE deposits in South China, as it could have provided favorable conditions for fluid circulation that would trigger alteration or dissolution of REE-bearing minerals in granites.

Alteration can transform primary REE-bearing minerals into the forms such as REE-fluorocarbonates that are easier to be weathered, which is important for the formation of ion-adsorption REE deposits (Ishihara et al. 2008; Imai et al. 2012; Bern et al. 2017; Zhao et al. 2022). For example, the Zhaibei granite that hosts an ion-adsorption LREE deposit is adjacent to the Zhuguangshan batholith; hydrothermal alteration has transformed its primary REE-bearing accessory minerals of titanite, allanite, monazite, and xenotime into REE-fluorocarbonates and thorite, which was important for ion-adsorption LREE mineralization (Zhao et al. 2022). In the Changjiang granite, allanite was partly replaced by REE-fluorocarbonates, and the occurrence of fracture-filling REE-fluorocarbonates (Figs. 4i, 5a-5h, and 7a) that represent the more easily weathered REE-minerals would set the stage for the formation of an ion-adsorption REE deposit (Ishihara et al. 2008; Rern et al. 2017). Furthermore, in the Changjiang granite, U and REE have also been released from uraninite during its alteration and dissolution (Zhang et al. 2021b); monazite was

DOI: https://doi.org/10.2138/am-2022-8531. http://www.minsocam.org/

partly replaced by apatite and an REE-rich phase during alteration (Fig. 3c). In contrast, alteration of allanite in the Jiufeng granite only generated minor REE-fluorocarbonates, and no obvious alteration was observed on other REE-bearing minerals such as titanite and thorite. Two ion-adsorption REE deposit have been found in the Zhuguangshan batholith (Fig. 1). Our study indicates that the Changjiang granite has potential to form an ion-adsorption LREE deposit, although further work needs to be done.

6. IMPLICATIONS

This study reports the first attempt to systematically investigate the textures and compositions of allanite during alteration from uranium-fertile and barren granites. Three major geological applications can be envisaged for the study of alteration and geochemistry of allanite.

Firstly, it may effectively elucidate the nature of a hydrothermal fluid from which allanite crystallized or that interacted with allanite. Textures and compositions of the Changjiang allanites combined with the occurrence of abundant fluorite suggest the presence of the superposition of F- and CO_2-bearing fluids with a relatively low-temperature (≤ 300 °C) and oxidized nature.

Secondly, U-Pb isotopes in allanite have been used to determine the ages of regional mineralization/hydrothermal events. Uranium-bearing accessory minerals such as uraninite, uranothorite, and allanite in granites generally represent the major sources of uranium for many hydrothermal uranium deposits; alteration of these minerals leading to uranium mobilization is important for the formation of hydrothermal uranium deposits (Cuney and Friedrich 1987; Chabiron et al. 2003; Cuney 2014; McGloin et al. 2016; Zhang et al. 2020b, 2021b). Dating altered domains of U-bearing accessory minerals can constrain connection with the timing of U mineralization or related hydrothermal events, which is important for understanding uranium mineralization processes. In this study, in situ U-Pb dating on the darker (secondary) domains of the Changjiang allanite grains yielded a weighted mean U-Pb age of 141.4 ± 5.6 Ma, consistent with the timing of a uranium mineralization event in the Changjiang uranium ore field (~140 Ma, Zhong et al. 2019) and the age of a crustal extension event (140−135 Ma) in South China (Li 2000; Hu et al. 2008). Our results provide temporal evidence for the link between uranium release from source rocks and regional crustal extension events in South China. In addition, this study also emphasizes the role of the regional crustal extension in the formation of ion-adsorption REE deposits in South China.

Thirdly, this study helps understand the mobilization processes of REE and U from primary minerals during alteration, usually a key step in the formation of an ion-adsorption REE deposit or a uranium deposit. Our study indicates that elemental maps obtained by EPMA and LA-ICP-MS can provide direct evidence for the microscale processes. This study suggests that allanite can be used as a useful tool for decoding granite-related uranium mineralization processes and can provide insights into the formation of ion-adsorption REE deposits.

ACKNOWLEDGEMENTS

This work was financially supported by the National Natural Science Foundation of China (grants 91962218, 42002077), the Fundamental Research Funds for the Central Universities (JZ2022HGTB0301), and the Fundamental Research Funds for Central Public Interest Scientific Institution (KK2011). We thank the staff of the Research Institute No. 290 of the China National Nuclear Corporation for their support during field work. We thank Xian Liang and Xiuling Du for their assistance with LA-ICP-MS analyses. The authors would like to thank Associate Editor Paul Tomascak and two anonymous reviewers for their constructive comments.

REFERENCES CITED

Bailey, E.H., and Ragnarsdottir, K.V. (1994) Uranium and thorium solubilities in subduction zone fluids. Earth and Planetary Science Letters, 124, 119–129.

Banks, D.A., Yardley, B.W.D., Campbell, A.R., and Jarvis, K.E. (1994) REE composition of an aqueous magmatic fluid: A fluid inclusion study from the Capitan Pluton, New Mexico, U.S.A. Chemical Geology, 113, 259–272.

Battaglia, S. (1999) Applying X-ray geothermometer diffraction to a chlorite. Clays and Clay Minerals, 47, 54–63.

Berger, A., Gnos, E., Janots, E., Fernandez, A., and Giese, J. (2008) Formation and composition of rhabdophane, bastnäsite and hydrated thorium minerals during alteration: Implications for geochronology and low-temperature processes. Chemical Geology, 254, 238–248.

Bern, C.R., Yesavage, T., and Foley, N.K. (2017) Ion-adsorption REEs in regolith of the Liberty Hill pluton, South Carolina, USA: An effect of hydrothermal alteration. Journal of Geochemical Exploration, 172, 29–40.

Bonnetti, C., Cuney, M., Bourlange, S., Deloule, E., Poujol, M., Liu, X.D., Peng, Y.B., and Yang, J.X. (2017) Primary uranium sources for sedimentary-hosted uranium deposits in NE China: insight from basement igneous rocks of the Erlian Basin. Mineralium Deposita, 52, 297–315.

Bonnetti, C., Liu, X.D., Mercadier, J., Cuney, M., Deloule, E., Villeneuve, J., and Liu, W.Q. (2018) The genesis of granite-related hydrothermal uranium deposits in the Xiazhuang and Zhuguang ore fields, North Guangdong Province, SE China: Insights from mineralogical, trace elements and U-Pb isotopes signatures of the U mineralization. Ore Geology Reviews, 92, 588–612.

Borst, A.M., Smith, M.P., Finch, A.A., Estrade, G., Villanova-de-Benavent, C., Nason, P., Marquis, E., Horsburgh, N.J., Googenough, K.M., Xu, C., Kynický, J., Geraki, K. (2020) Adsorption of rare earth elements in regolith-hosted clay deposits. Nature Communications, 11, 1−15.

Chabiron, A., Cuney, M., and Poty, B. (2003) Possible uranium sources for the largest uranium district associated with volcanism: the Streltsovka caldera (Transbaikalia, Russia). Mineralium Deposita, 38, 127−140.

Chen, W.T., and Zhou, M. (2014) Ages and compositions of primary and secondary allanite from the Lala Fe–Cu deposit, SW China: implications for multiple episodes of hydrothermal events. Contributions to Mineralogy and Petrology, 168, 1043–1062.

Chen, Y.W., Bi, X.W., Hu, R.Z., and Dong, S.H. (2012) Element geochemistry, mineralogy, geochronology and zircon Hf isotope of the Luxi and Xiazhuang granites in Guangdong province, China: implications for U mineralization. Lithos, 150, 119–134.

Chi, G.X., Ashton, K., Deng, T., Xu, D.R., Li, Z.H., Song, H., Liang, R., and Kennicott, J. (2020) Comparison of granite-related uranium deposits in the Beaverlodge district (Canada) and

South China–a common control of mineralization by coupled shallow and deep-seated geologic processes in an extensional setting. Ore Geology Reviews, 117, 103319.

Cuney, M. (2009) The extreme diversity of uranium deposit. Mineralium Deposita, 44, 3–9.

Cuney, M. (2014) Felsic magmatism and uranium deposits. Bulletin de la Société Géologique de France, 185, 75–92.

Cuney, M., and Friedrich, M. (1987) Physicochemical and crystal-chemical controls on accessory mineral paragenesis in granitoids: implications for uranium metallogenesis. Bulletin de Minéralogy, 110, 235–247.

Darling, J.R., Storey, C.D., and Engi, M. (2012) Allanite U–Th–Pb geochronology by laser ablation ICPMS. Chemical Geology, 292, 103–115.

Dahlkamp, F.J. (2009) Uranium Deposits of the World: Asia. Berlin, Heidelberg: Springer-Verlag, 493 p.

Deer, W.A., Howie, R.A., and Zussman, J. (1986) Rock-forming minerals. Volume 1B. Disilicates and Ring silicates, 2nd ed, p. 629, Longman, London and New York.

Deng, P., Ren, J.S., Ling, H.F., Shen, W.Z., Sun, L.Q., Zhu, B., and Tan, Z.Z. (2012) SHRIMP zircon U-Pb ages and tectonic implications for Indosinian granitoids of southern Zhuguangshan granitic composite, South China. Chinese Science Bulletin, 57, 1542–1552.

Deng, X.D., Li, J.W., and Wen, G. (2014) Dating iron skarn mineralization using hydrothermal allanite-(La) U-Th-Pb isotopes by laser ablation ICP-MS. Chemical Geology, 382, 95–110.

Fu, W., Li, X.T., Feng, Y.T., Feng, M., and Lin, H. (2019) Chemical weathering of S-type granite and formation of Rare Earth Element (REE)-rich regolith in South China: Critical control of lithology. Chemical Geology, 520, 33–51.

Gieré, R., and Sorensen, S.S. (2004) Allanite and other REE-rich epidotegroup minerals, in Liebscher, A., and Franz, G., eds., Epidotes. Reviews in Mineralogy and Geochemisty, 56, 431–493.

Gregory, C.J., Rubatto, D., Allen, C. M., Williams, I.S., Hermann, J., and Ireland, T. (2007) Allanite micro-geochronology: A LA-ICP-MS and SHRIMP U–Th–Pb study. Chemical Geology, 245, 162–182.

Hu, H., Wang, R.C., Chen, W.F., Chen, P.R., Ling, H.F., and Liu, G.N. (2013) Timing of hydrothermal activity associated with the Douzhashan uranium-bearing granite and its significance for uranium mineralization in northeastern Guangxi, China. Chinese Science Bulletin, 58, 4319–4328.

Hu, R.Z., and Jin, J.F. (1990) Mechanism of the migration and deposition of uranium in ascending hydrothermal solutions-Evidence from the Xiwang uranium deposit. Geological Review, 36, 317-325 (in Chinese with English abstract).

Hu, R.Z., Bi, X.W., Su, W.C., Peng, J.T., and Li, C.Y. (2004) The relationship between uranium metallogenesis and crustal extension during the Cretaceous-Tertiary in South China. Earth Science Frontiers, 11, 153−160 (in Chinese with English abstract).

Hu, R.Z., Bi, X.W., Zhou, M.F., Peng, J.T., Su, W.C., Liu, S., and Qi, H.W. (2008) Uranium metallogenesis in South China and its relationship to crustal extension during the Cretaceous to Tertiary. Economic Geology, 103, 583−598.

Huang, J., Tan, W., Liang, X., He, H., Ma, L., Bao, Z., and Zhu, J. (2021) REE fractionation controlled by REE speciation during formation of the Renju regolith-hosted REE deposits in Guangdong Province, South China. Ore Geology Reviews, 134, 104172.

Imai, A., Yonezu, K., Sanematsu, K., Ikuno, T., Ishida, S., Watanabe, K., Pisutha-Arnond, V., Nakapadungrat, S., and Boosayasak, J. (2013) Rare earth elements in hydrothermally altered granitic rocks in the Ranong and Takua Pa Tin-Field, Southern Thailand. Resource Geology, 63, 84–98.

Ishihara, S., Hua, R., Hoshino, M., and Murakami, H. (2008) REE abundance and REE minerals in granitic rocks in the Nanling Range, Jiangxi province, southern China, and generation of the REE-rich weathered crust deposits. Resource Geology, 58, 355–372.

Jackson, S.E., Pearson, N.J., Griffin, W.L., and Belousova, E.A. (2004) The application of laser ablation-inductively coupled plasma-mass spectrometry to in situ U–Pb zircon geochronology. Chemical Geology, 211, 47–69.

Keppler, H., and Wyllie, P.J. (1990) Role of fluids in transport and fractionation of uranium and thorium in magmatic processes. Nature, 348, 531−533.

Kynicky, J., Smith, M.P., and Xu, C. (2012) Diversity of rare earth deposits: The key example of China. Elements, 8, 361−367.

Langmuir, D. (1978) Uranium solution-mineral equilibria at low temperatures with applications to sedimentary ore deposits. Geochimica et Cosmochimica Acta, 42, 547−569.

Li, X.H. (2000) Cretaceous magmatism and lithospheric extension in Southeast China. Journal of Asian Earth Sciences, 18, 293–305.

Li, X.H., and McCulloch, M.T. (1998) Geochemical characteristics of Cretaceous mafic dikes from northern Guangdong, SE China: Age, origin and tectonic significance, in Flower, M.F.J., Chung, S.L., Lo, C.H., and Lee, T.Y., eds., Mantle Dynamics and Plate Interaction in East Asia, Geodynamics 27, American Geophysical Union, Washington D.C., p. 405–419.

Li, Y.H.M., Zhao, W.W., and Zhou, M.F. (2017) Nature of parent rocks, mineralization styles and ore genesis of regolith-hosted REE deposits in South China: An integrated genetic model. Journal of Asian Earth Sciences, 148, 65–95.

Li, M.Y.H., Zhou, M.F., and Williams-Jones, A.E. (2019) The Genesis of Regolith-Hosted Heavy Rare Earth Element Deposits: Insights from the World-Class Zudong Deposit in Jiangxi Province, South China. Economic Geology, 114, 541–568.

Liao, X., Li, Q.L., Whitehouse, M.J., Yang, Y.H., and Liu, Y. (2020) Allanite U–Th–Pb geochronology by ion microprobe. Journal of Analytical Atomic Spectrometry, 35, 489–497.

Littlejohn, A.L. (1981) Alteration products of accessory allanite in radioactive granites from the Canadian Shield. Papers Geological Survey of Canada 81-1B, p. 95–104.

Luo, J.C., Hu, R.Z., Fayek, M., Li, C.S., Bi, X.W., Abdu, Y., and Chen, Y.W. (2015) In-situ SIMS uraninite U-Pb dating and genesis of the Xianshi granite-hosted uranium deposit, South China. Ore Geology Reviews, 65, 968–978.

Mao, J.W., Chen, Y.B., Chen, M.H., and Franco, P. (2013) Major types and time–space distribution of Mesozoic ore deposits in South China and their geodynamic settings. Mineralium Deposita, 48, 267–294.

McFarlane, C.R.M. (2016) Allanite U-Pb geochronology by 193nm LA ICP-MS using NIST610 glass for external calibration. Chemical Geology, 438, 91–102.

McGloin, M.V., Tomkins, A.G., Webb, G.P., Spiers, K., MacRae, C.M., Paterson, D., and Ryan, C.G., 2016, Release of uranium from highly radiogenic zircon through metamictization: The source of orogenic uranium ores. Geology, 44, 15–18.

Middleton, A.W., Förster, H.J., Uysal, I.T., Golding, S.D., and Rhede, D. (2013) Accessory phases from the Soultz monzogranite, Soultz-sous-Forêts, France: implications for titanite destabilisation and differential REE, Y and Th mobility in hydrothermal systems. Chemical Geology, 335, 105–117.

Migdisov, A., Williams-Jones, A.E., Brugger, J., and Caporuscio, F.A. (2016) Hydrothermal transport, deposition, and fractionation of the REE: Experimental data and thermodynamic calculations. Chemical Geology, 439, 13–42.

Min, M.Z., Luo, X.Z., Du, G.S., He, B.A., and Campbell, A.R. (1999) Mineralogical and geochemical constraints on the genesis of the granite-hosted Huangao uranium deposit, SE China. Ore Geology Reviews, 14, 105–127.

Morin, J.A. (1977) Allanite in granitic rocks of the Kenora-Vermilion Bay area, northwestern Ontario. The Canadian Mineralogist, 15, 297–302.

Ngo, X.D., Zhao, X.F., Tran, T.H., Deng, X.D., and Li, J.W. (2020) Two episodes of REEs mineralization at the Sin Quyen IOCG deposit, NW Vietnam. Ore Geology Reviews, 125, 103676.

Pal, D.C., Chaudhuri, T., Mcfarlane, C.R., Mukherjee, A., and Sarangi, A.K. (2011) Mineral chemistry and in situ dating of allanite, and geochemistry of its host rocks in the Bagjata uranium Mine, Singhbhum Shear Zone, India—Implications for the chemical evolution of REE mineralization and mobilization. Economic Geology, 106, 1155–1171.

Petrík, I., Broska, I., Lipka, J., and Siman, P. (1995) Granitoid allanite-(Ce): Substitution relations, redox conditions and REE distributions (On an example of I-type granitoids, western Carpathians, Slovakia). Geologica Carpathica, 46, 79–94.

Poitrasson, F. (2002) In situ investigations of allanite hydrothermal alteration: examples from calc-alkaline and anorogenic granites of Corsica (southeast France). Contributions to Mineralogy and Petrology, 142, 485–500.

Romberger, S.B. (1984) Transport and deposition of uranium in hydrothermal systems at temperatures up to 300 °C: geological implications, *in* De Vivo, B., Ippolito, F., Capaldi, G., and Simpson. P.R., eds., Uranium geochemistry, mineralogy, geology, exploration and resources. The Institute of Mining and Metallurgy, London, p. 12−17.

Ruzicka, V. (1993) Vein uranium deposits. Ore Geology Reviews, 8, 247–276.

Skrzypek, E., Sakata, S., and Sorger, D. (2020) Alteration of magmatic monazite in granitoids from the Ryoke belt (SW Japan): Processes and consequences. American Mineralogist, 10, 538–554.

Smith, M.R., Henderson, P., and Jeffries, T. (2002) The formation and alteration of allanite in skarn from the Beinn an Dubhaich granite aureole, Skye. European Journal of Mineralogy, 14, 471–486.

Smye, A.J., Roberts, N.M.W., Condon, D.J., Horstwood, M.S.A., and Parrish, R.R. (2014) Characterising the U–Th–Pb systematics of allanite by ID and LA-ICPMS: Implications for geochronology. Geochimica et Cosmochimica Acta, 135, 1–28.

Sun, S.S., and McDonough, W.F. (1989) Chemical and isotopic systematics of oceanic basalts: Implications for mantle composition and processes, *in* Sanders, A.D., and Norry, M.J., eds., Magmatism in the Ocean Basins: Geological Society of London, Special Publication, 42, 313−345.

Uher, P., Ondrejka, M., Bačík. P., Broska, I,, and Konečný, P. (2015) Britholite, monazite, REE carbonates, and calcite: Products of hydrothermal alteration of allanite and apatite in A-type granite from Stupné, Western Carpathians, Slovakia. Chemical Geology, 236–237, 212–225.

Walters, A.S., Goodenough, K.M., Hughes, H., Roberts, N., Gunn, A.G., Rushton, J., and Lacinska, L. (2013) Enrichment of rare earth elements during magmatic and post-magmatic processes: a case study from the Loch Loyal Syenite Complex, northern Scotland. Contributions to Mineralogy and Petrology, 166, 1177–1202.

Wang, F.Y., Ge, C., Ning, S.Y., Nie, L.Q., Zhong, G.X., and White, N.C. (2017) A new approach to LA-ICP-MS mapping and application in geology. Acta Petrologica Sinica, 33, 3422–3436 (in Chinese with English abstract).

Wiedenbeck, M., Allé, P., Corfu, F., Griffin, W.L., Meier, M., Oberli, F., Von Quadt, A., Roddick, J., and Spiegel, W. (1995) Three natural zircon standards for U-Th-Pb, Lu-Hf, trace element and REE analyses. Geostandards Newsletter, 19, 1–23.

Wood, S.A. (1990) The aqueous geochemistry of the rare-earth elements and yttrium: 2. Theoretical predictions of speciation in hydrothermal solutions to 350 °C at saturation water vapor pressure. Chemical Geology, 88, 99–125.

Wood, S.A., and Ricketts, A. (2000) Allanite-(Ce) from the Eocene Casto granite, Idaho: Response to hydrothermal alteration. The Canadian Mineralogist, 38, 81–100.

Wu, C., Huang, D., Guo, Z. (1990). REE geochemistry in the weathered crust of granites, Longnan area, Jiangxi Province. Acta Geologica Sinica (English Edition), 3, 193–209.

Xie, Y., Hou, Z., Goldfarb, R.J., Guo, X., and Wang, L. (2016) Rare earth element deposits in China. Reviews in Economic Geology, 18, 115c136.

Zhang, B.T. (1990) Endogenic uranium deposits and methods of study. Beijing: Atomic Energy Press, 1–538 (in Chinese).

Zhang, C., Cai, Y., Xu, H., Dong, Q., Liu, J., and Hao, R. (2017a) Mechanism of mineralization in the Changjiang uranium ore field, South China: evidence from fluid inclusions, hydrothermal alteration, and H–O isotopes. Ore Geology Reviews, 86, 225–253.

Zhang, C., Cai, Y.Q., Dong, Q., and Xu, H. (2020a) Cretaceous–Neogene basin control on the formation of uranium deposits in South China: evidence from geology, mineralization ages, and H–O isotopes. International Geology Review, 62, 263–310.

Zhang, L., Chen, Z.Y., Li, S.R., Santosh, M., Huang, G.L., and Tian, Z.J. (2017b) Isotope geochronology, geochemistry, and mineral chemistry of the U-bearing and barren granites from the Zhuguangshan complex, South China: Implications for petrogenesis and uranium mineralization. Ore Geology Reviews, 91, 1040–1065.

Zhang, L., Chen, Z.Y., Li, X.F., Li, S.R., Santosh, M., and Huang, G.L. (2018a) Zircon U-Pb geochronology and geochemistry of granites in the Zhuguangshan complex, South China: Implications for uranium mineralization. Lithos, 308–309, 19–33.

Zhang, L., Chen, Z.Y., Li, S.R., and Huang, G.L. (2018b) Characteristics of uranium minerals in wall-rock alteration zones from the Mianhuakeng (No. 302) uranium deposit, northern Guangdong, South China. Acta Petrologica Sinica, 35, 2657–2670 (in Chinese with English abstract).

Zhang, L., Li, X.F., Wang, G., and Wang, M. (2020b) Direct evidence for the source of uranium in the Baiyanghe deposit from accessory mineral alteration in the Yangzhuang granite porphyry, Xinjiang Province, Northwest China. American Mineralogist, 105, 1556–1571.

Zhang, L., Chen, Z.Y., Wang, F.Y., and Zhou, T.F. (2021a) Whole-rock and biotite geochemistry of granites from the Miao'ershan batholith, South China: Implications for the sources of granite-hosted uranium ores. Ore Geology Reviews, 129, 103930.

Zhang, L., Chen, Z.Y., Fang, Y.W., White, N.C., and Zhou, T.F. (2021b) Release of uranium from uraninite in granites through alteration: Implications for the source of granite-related uranium ores. Economic Geology, 116, 1115–1139.

Zhang, Z.H., and Zhang, B.T. (1991) On the Uranium-bearing granites and their related uranium deposits in South China. Atomic Energy Press, Beijing, pp. 1–258 (in Chinese).

Zhao, K.D., Jiang, S.Y., Dong, C.Y., Chen, W.F., Chen, P.R., Ling, H.F., Zhang, J., and Wang, K.X. (2011) Uranium-bearing and barren granites from the Taoshan complex, Jiangxi province, South China: geochemical and petrogenetic discrimination and exploration significance: Journal of Geochemical Exploration, 110, 126–135.

Zhao, K.D., Jiang, S.Y., Ling, H.F., Sun, T., Chen, W.F., Chen, P.R., and Pu, W. (2016) Late Triassic U-bearing and barren granites in the Miao'ershan batholith, South China: Petrogenetic discrimination and exploration significance. Ore Geology Reviews, 77, 260–278.

Zhao, Z., Wang, D., Bagas, L., and Chen, Z. (2022) Geochemical and REE mineralogical characteristics of the Zhaibei Granite in Jiangxi Province, southern China, and a model for the genesis of ion-adsorption REE deposits. Ore Geology Reviews, 140, 104579.

Zhong, F.J., Yan, J., Xia, F., Pan, J.Y., Liu, W.Q., Lai, J., and Zhao, Q.F. (2019) In-situ U-Pb isotope geochronology of uraninite for Changjiang granite-type uranium ore field in northern Guangdong, China: Implications for uranium mineralization. Acta Petrologica Sinica, 35, 2727–2744 (in Chinese with English abstract).

Zhou, X.M., Sun, T., Shen, W.Z., Shu, L.S., and Niu, Y.L. (2006) Petrogenesis of Mesozoic granitoids and volcanic rocks in South China: a response to tectonic evolution. Episodes, 29, 26–33.

Figure captions

Figure 1. A simplified geological map of South China showing the distribution of granites of different ages, granite-related uranium deposits, and ion-adsorption REE deposits (modified from Zhou et al. 2006; Hu et al. 2008; Li et al. 2017).

Figure 2. Simplified geologic map of the Zhuguangshan batholith showing the distribution of the main granite-related uranium deposits (modified from Deng et al. 2012; Zhang et al. 2018a; Zhong et al. 2019).

Figure 3. Representative transmitted polarized light and BSE images of the Changjiang and Jiufeng granites and uranium ores. (**a**) Transmitted polarized light image showing that the alteration minerals in the samples collected from the Changjiang granite include chlorite and illite. Allanite is spatially associated with biotite. (**b-c**) BSE images of uraninite and monazite in the samples collected from the Changjiang granite. Monazite was partly replaced by apatite and REE-rich phase. (**d**) Transmitted polarized light image showing that allanite in the Jiufeng granite is euhedral and shows little sign of alteration. (**e-f**) BSE images of quartz, fluorite, pitchblende, pyrite, and sericite in uranium ores of the 302 deposit. Mineral abbreviations: Aln = allanite; Ap = apatite; Bt = biotite; Chl = chlorite; Fl = fluorite; Mnz = monazite; Pit = pitchblende; Py = pyrite; Qz = quartz; Ser = sericite; Urn = uraninite.

Figure 4. Representative BSE images of allanites from the Changjiang (**a-f**) and

DOI: https://doi.org/10.2138/am-2022-8531. http://www.minsocam.org/

Jiufeng (**g-l**) granites. These allanite grains show two different types of domains that are characterized by different levels of grey: brighter, interpreted as primary magmatic allanite, and darker, representing secondary allanite. Some REE-rich microveinlets are present in the grain boundaries or micro-cracks within rock-forming minerals such as feldspars and quartz. Mineral abbreviations: Aln = allanite; Ap = apatite; Bt = biotite; Chl = chlorite; Kfs = K-feldspar; Mag = magnetite; Pl = plagioclase; Qz = quartz.

Figure 5. Representative BSE images of altered allanites from the Changjiang granite. (**a-l**) Allanite grains were partly replaced by REE-fluorocarbonates, calcite, fluorite, thorite, clay minerals, quartz, TiO_2, and epidote. REE-rich microveinlets are present in the grain boundaries or micro-cracks within rock-forming minerals and they are shown as differing grey levels under BSE imaging. Mineral abbreviations: Aln = allanite; Ap = apatite; Chl = chlorite; Ep = epidote; Fl = fluorite; Kfs = K-feldspar; Pl = plagioclase; Qz = quartz; Thr = thorite; Zrn = zircon.

Figure 6. Element maps obtained by EPMA of an altered allanite grain from the Changjiang granite showing the proposed mobilization and reprecipitation of La, Ce, Th, and U.

Figure 7. Element maps obtained by LA-ICP-MS of an altered allanite grain from the Changjiang granite showing the distributions of Ca, Fe, U, and REE.

Figure 8. (**a**) The BSE image showing the EPMA spot positions in the Jiufeng allanite grain from Fig. 4g. (**b-c**) Profile variations of Al, Ca, ΣREE, Fe^{3+}, Th, and Pb

concentrations. (**d**) Cationic contents in the A and M sites.

Figure 9. Plot of ΣREE vs. Al for allanites from the Changjiang and Jiufeng granites (after Petrík et al. 1995).

Figure 10. Chondrite-normalized REE patterns of brighter and darker domains of the Changjiang (**a-b**) and Jiufeng (**c-d**) allanite grains. Values of chondrite were taken from Sun and MacDonough (1989).

Figure 11. U-Pb concordia diagrams with representative CL images of zircons from the Changjiang (**a**) and Jiufeng (**b**) granites.

Figure 12. U-Pb Tera-Wasserburg concordia diagrams and ^{207}Pb corrected ^{206}Pb-^{238}U weighted ages for the brighter (**a-b**) and darker (**c-d**) domains of the Changjiang allanite grains and those for brighter domains of the Jiufeng allanite grains (**e-f**).

Figure 13. Diagrams illustrating potential elemental substitution mechanisms for the Changjiang (**a**) and Jiufeng (**b**) allanites. (**a**) $La^{3+} + Ce^{3+} + Fe^{2+} + Fe^{3+}$ vs. $Si^{4+} + Th^{4+} + Al^{3+}$. (**b**) $REE^{3+} + Fe^{2+}$ vs. $Ca^{2+} + Fe^{3+}$.

Figure 14. LogfO_2 vs. pH diagram showing the fluid evolution path in the Changjiang uranium ore field (after Romberger 1984). The heavy dashed lines show the boundaries between the stability fields for the various uranium complexes and various iron solids and aqueous species. The boundary that expresses the relative stability of bornite and chalcopyrite is shown as a fine dashed line. The light dot-dashed lines show the boundaries between the stability fields for the potassium silicates, kaolinite, alunite, sericite and adularia. The boundaries between the fields for the magnesium silicates chlorite and magnesian

montmorillonite are shown as light double-dot-dashed lines. Area I would be a low fO_2 and pH assemblage characterized by either alunite or kaolinite alteration. Mineral assemblages in Area II will be characterized by argillic alteration (kaolinite and/or montmorillonite) accompanied by hematite and/or iron carbonate. Area III lies within the sericite and chlorite stability fields. Area A represents the possible fO_2 and pH conditions of alteration of the allanite-bearing Changjiang granite. Area B represents the physicochemical conditions of precipitation of uranium from ore-forming fluids in the 302 deposit.

Supplementary Table captions

Supplementary Table S1 EPMA chemical compositions (wt%) and formulae of allanites from the Changjiang and Jiufeng granites.

Supplementary Table S2 LA-ICP-MS elemental data (ppm) of allanites from the Changjiang and Jiufeng granites.

Supplementary Table S3 EPMA chemical compositions (wt%) of alteration products (including REE-fluorocarbonates, thorite, and chlorite) of the Changjiang allanites.

Supplementary Table S4 LA-ICP-MS U-Pb isotopic data for zircons from the Changjiang and Jiufeng granites.

Supplementary Table S5 LA-ICP-MS U-Pb isotopic data for allanites from the Changjiang and Jiufeng granites.

This is the peer-reviewed, final accepted version for American Mineralogist, published by the Mineralogical Society of America.
The published version is subject to change. Cite as Authors (Year) Title. American Mineralogist, in press.
DOI: https://doi.org/10.2138/am-2022-8531. http://www.minsocam.org/

Figure 1

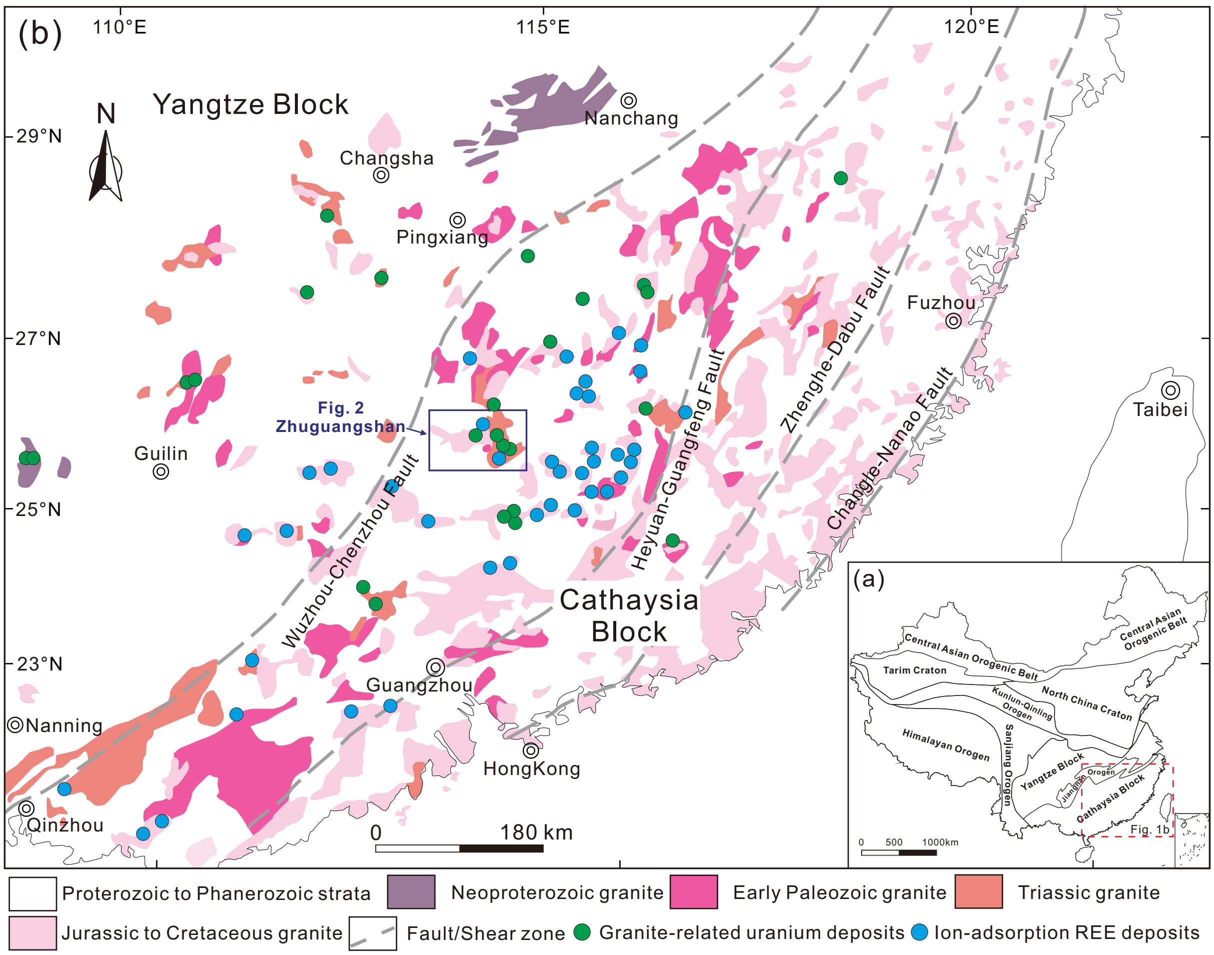

Figure 2

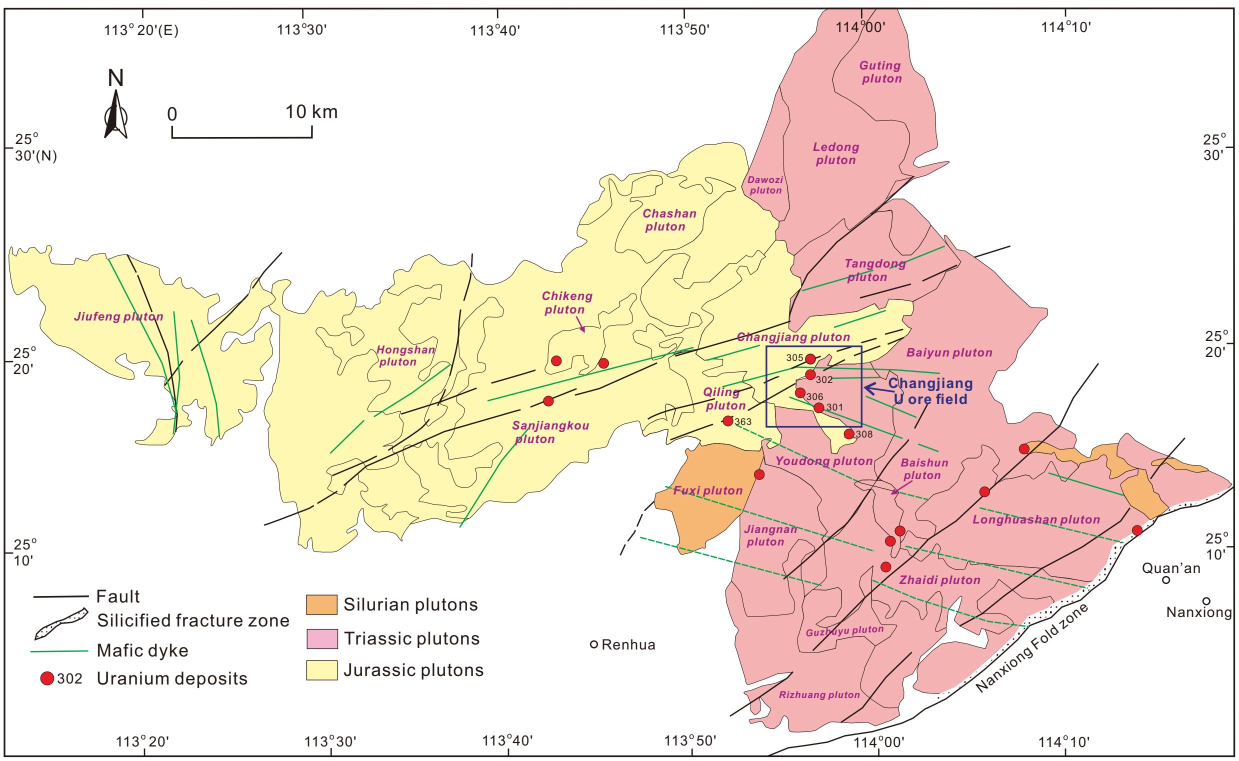
113° 20'(E)
113°30'
113°40'
113°50'
114°00'
114°10'
N
0
10 km
25° 30'(N)
25° 30'
25° 20'
25° 10'
Guting pluton
Ledong pluton
Dawozi pluton
Chashan pluton
Tangdong pluton
Jiufeng pluton
Chikeng pluton
Hongshan pluton
Changjiang pluton
Baiyun pluton
Changjiang U ore field
Qiling pluton
Sanjiangkou pluton
305
302
306
301
308
363
Youdong pluton
Baishun pluton
Fuxi pluton
Longhuashan pluton
Jiangnan pluton
Zhaidi pluton
Guzhuyu pluton
Rizhuang pluton
Quan'an
Nanxiong
Nanxiong Fold zone
Renhua
Fault
Silicified fracture zone
Mafic dyke
302 Uranium deposits
Silurian plutons
Triassic plutons
Jurassic plutons
113° 20'
113°30'
113°40'
113°50'
114°00'
114°10'

This is the peer-reviewed, final accepted version for American Mineralogist, published by the Mineralogical Society of America.
The published version is subject to change. Cite as Authors (Year) Title. American Mineralogist, in press.
DOI: https://doi.org/10.2138/am-2022-8531. http://www.minsocam.org/

Figure 3

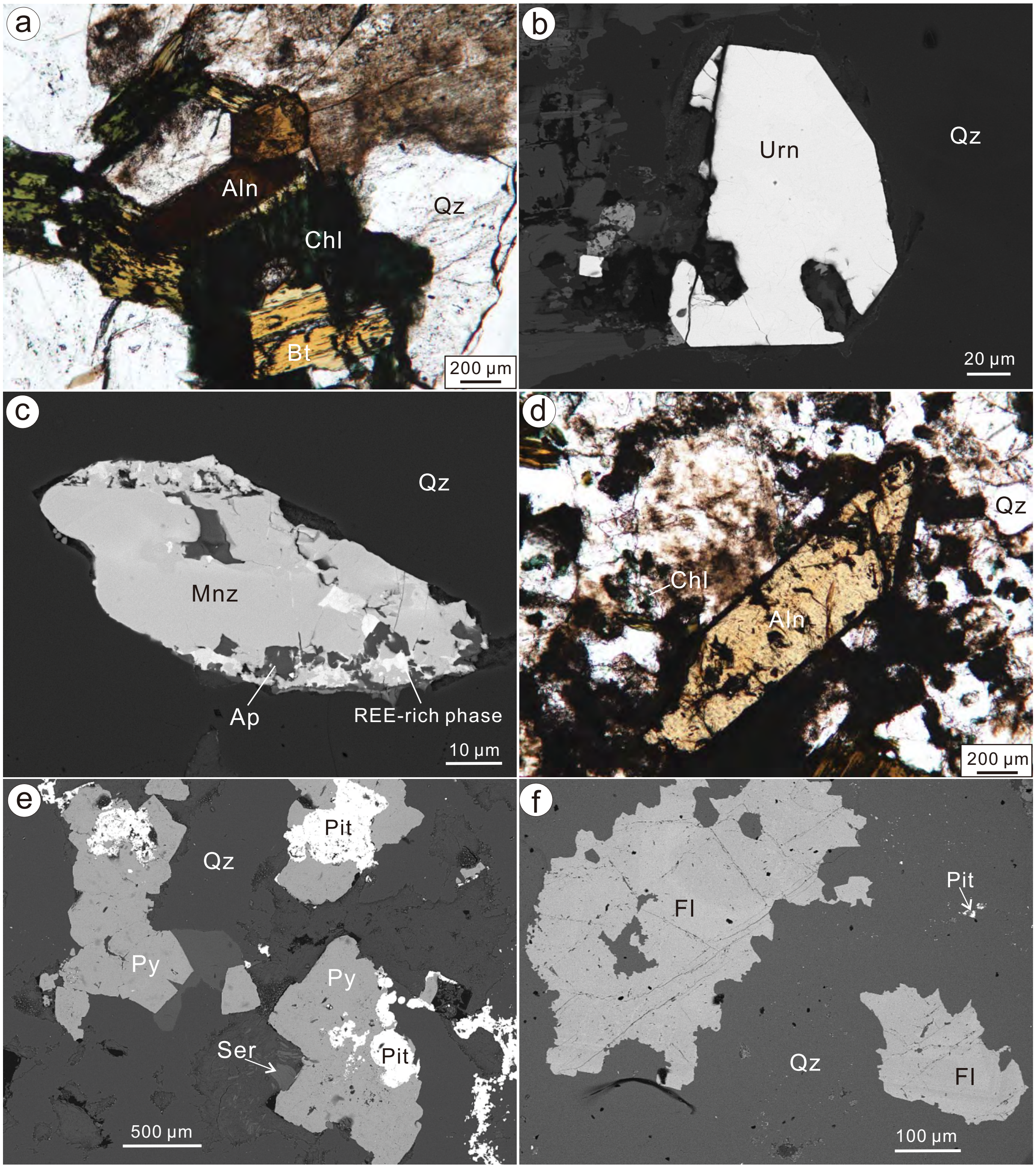

This is the peer-reviewed, final accepted version for American Mineralogist, published by the Mineralogical Society of America.
The published version is subject to change. Cite as Authors (Year) Title. American Mineralogist, in press.
DOI: https://doi.org/10.2138/am-2022-8531. http://www.minsocam.org/

Figure 4

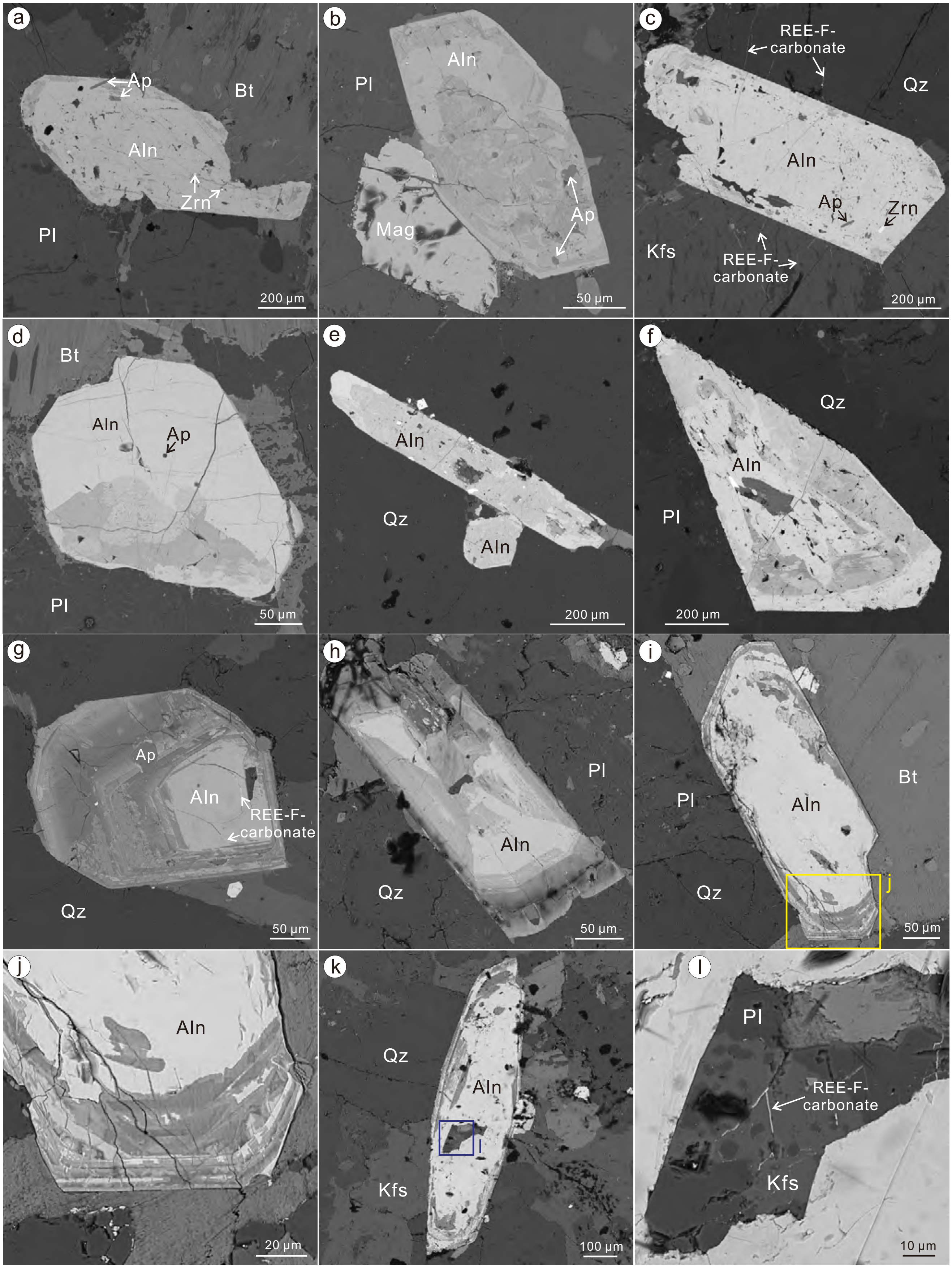

This is the peer-reviewed, final accepted version for American Mineralogist, published by the Mineralogical Society of America.
The published version is subject to change. Cite as Authors (Year) Title. American Mineralogist, in press.
DOI: https://doi.org/10.2138/am-2022-8531. http://www.minsocam.org/

Figure 5

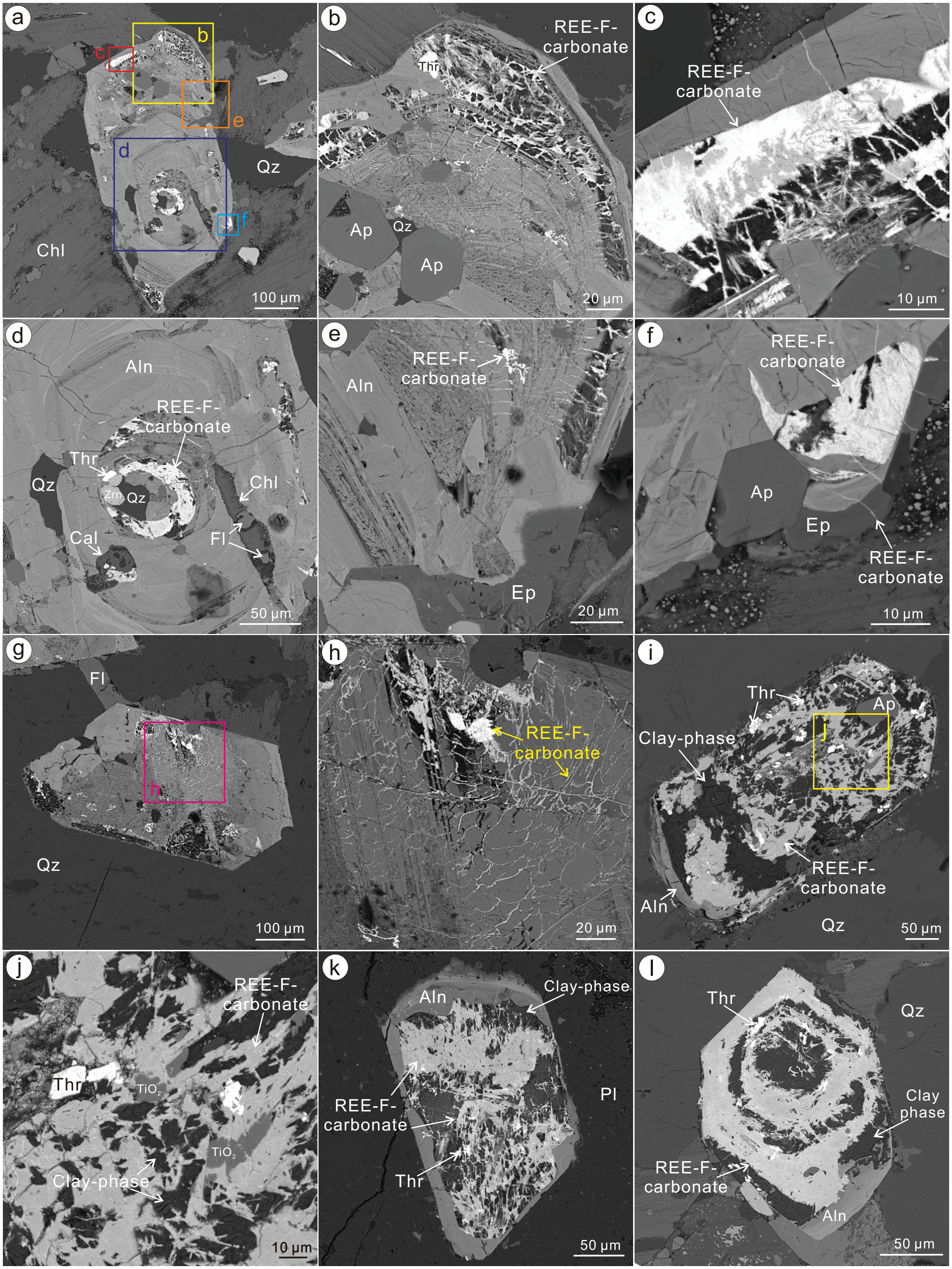

This is the peer-reviewed, final accepted version for American Mineralogist, published by the Mineralogical Society of America.
The published version is subject to change. Cite as Authors (Year) Title. American Mineralogist, in press.
DOI: https://doi.org/10.2138/am-2022-8531. http://www.minsocam.org/

Figure 6

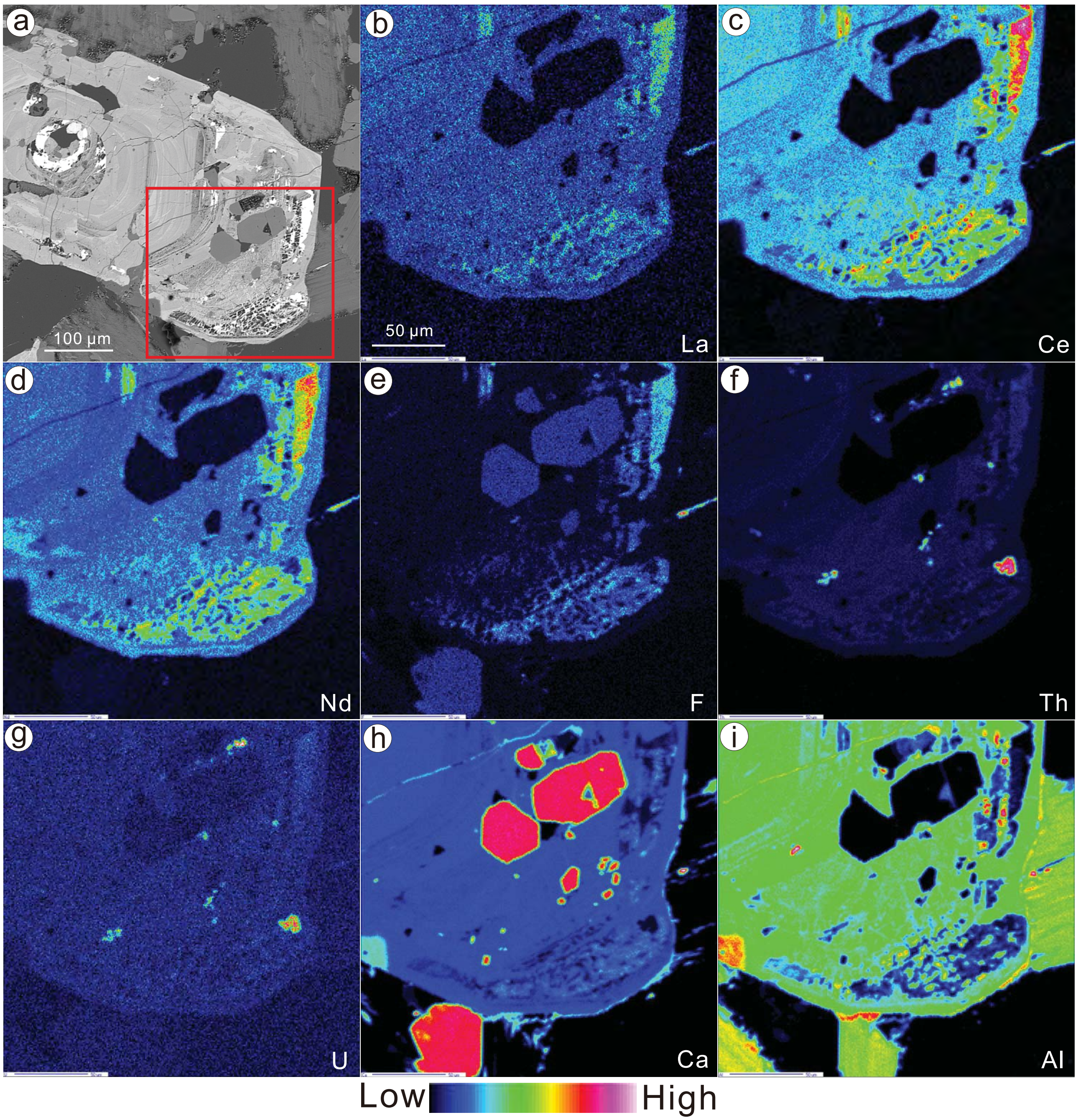

This is the peer-reviewed, final accepted version for American Mineralogist, published by the Mineralogical Society of America.
The published version is subject to change. Cite as Authors (Year) Title. American Mineralogist, in press.
DOI: https://doi.org/10.2138/am-2022-8531. http://www.minsocam.org/

Figure 7

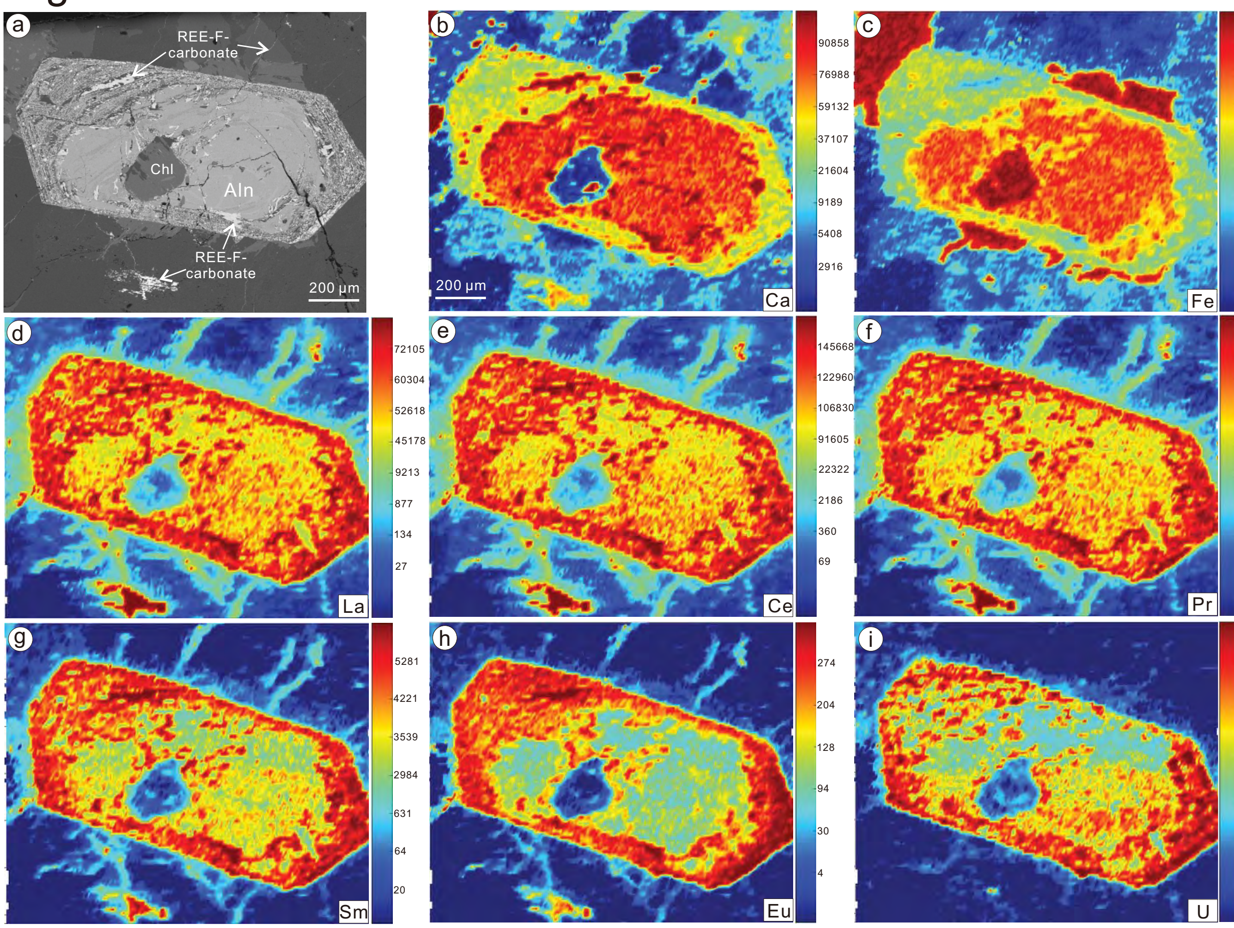

Figure 8

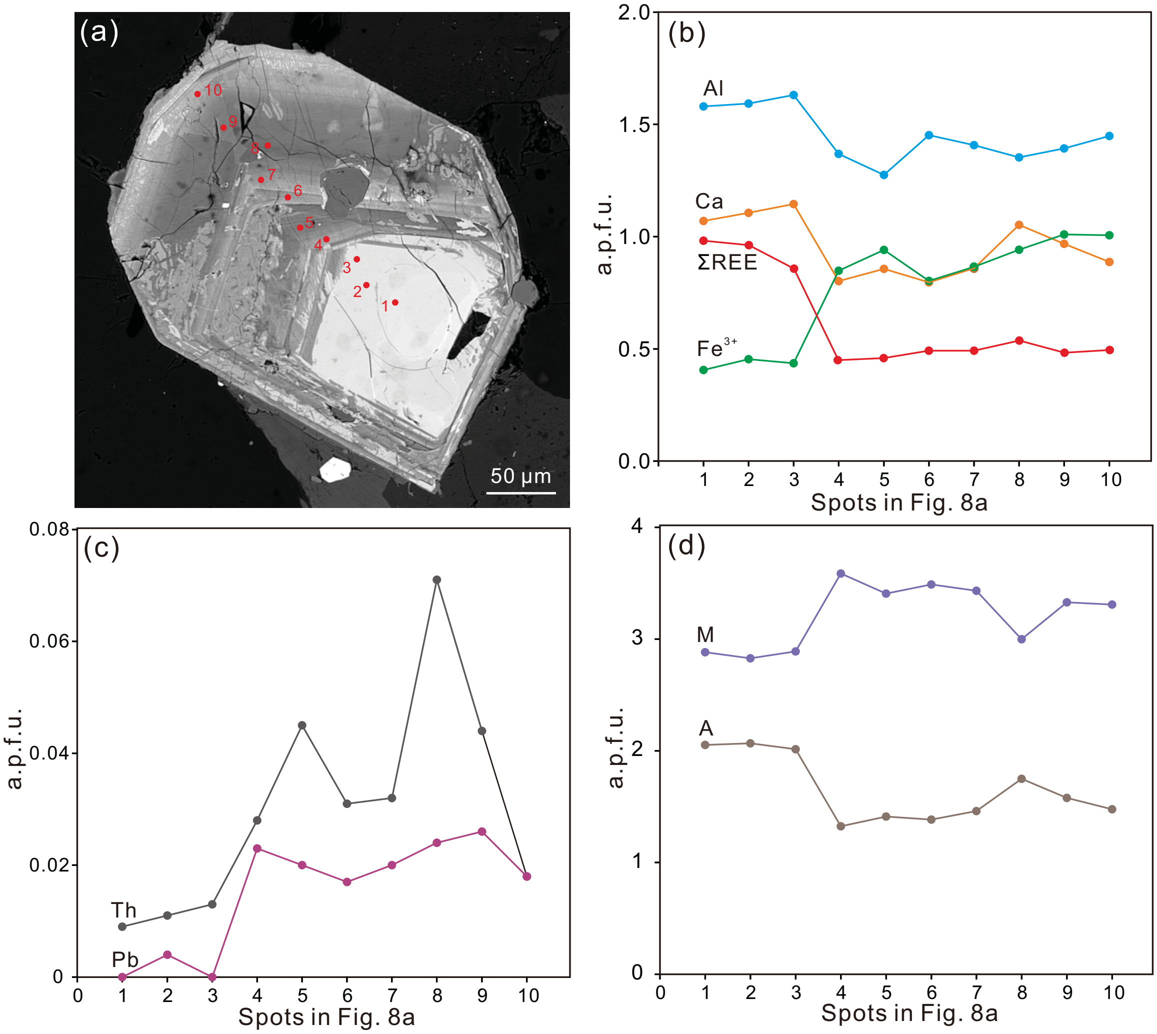
(a)
10
9
8
7
6
5
4
3
2
1
50 μm
(b)
2.0
1.5
1.0
0.5
0.0
Al
Ca
ΣREE
Fe3+
a.p.f.u.
1 2 3 4 5 6 7 8 9 10
Spots in Fig. 8a
(c)
0.08
0.06
0.04
0.02
0
Th
Pb
a.p.f.u.
0 1 2 3 4 5 6 7 8 9 10
Spots in Fig. 8a
(d)
4
3
2
1
0
M
A
a.p.f.u.
0 1 2 3 4 5 6 7 8 9 10
Spots in Fig. 8a

DOI: https://doi.org/10.2138/am-2022-8531. http://www.minsocam.org/

Figure 9

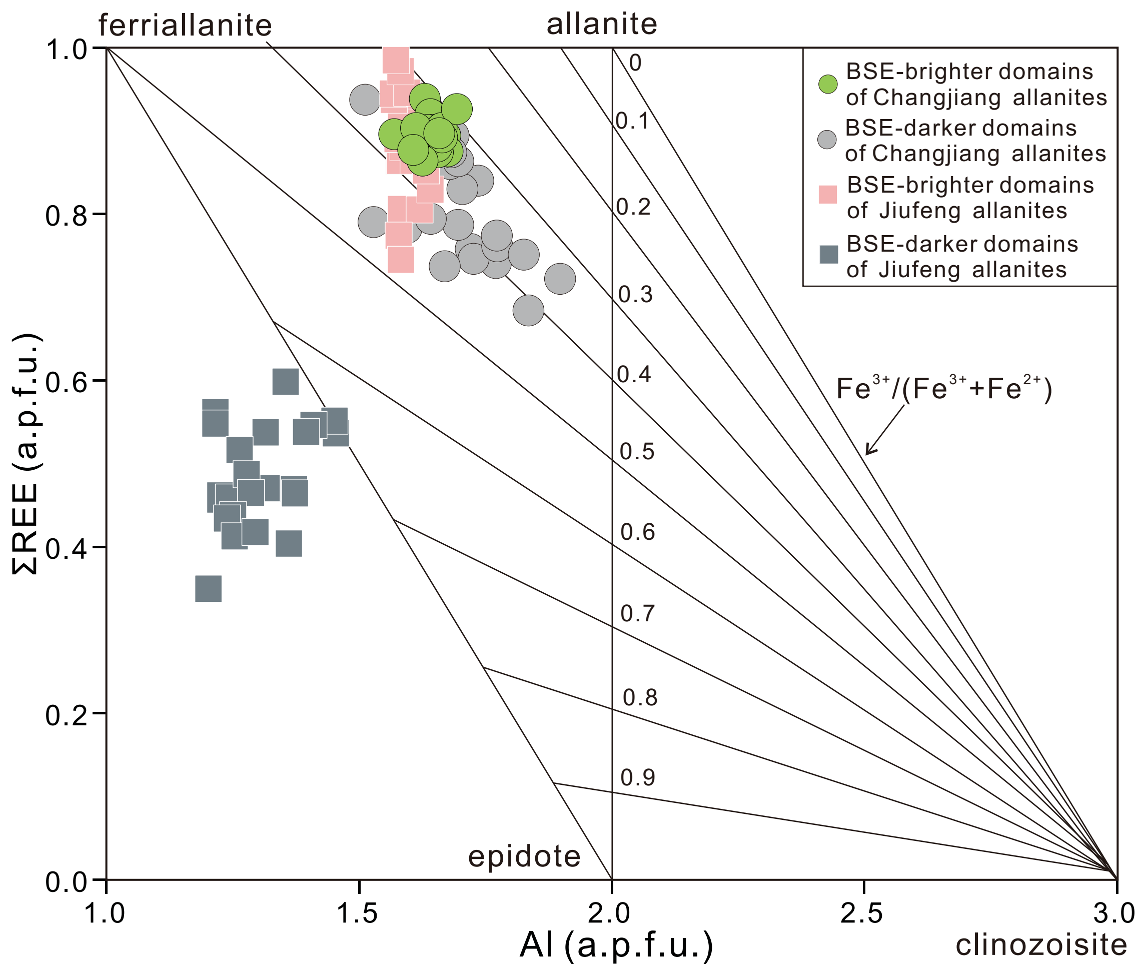

Figure 10

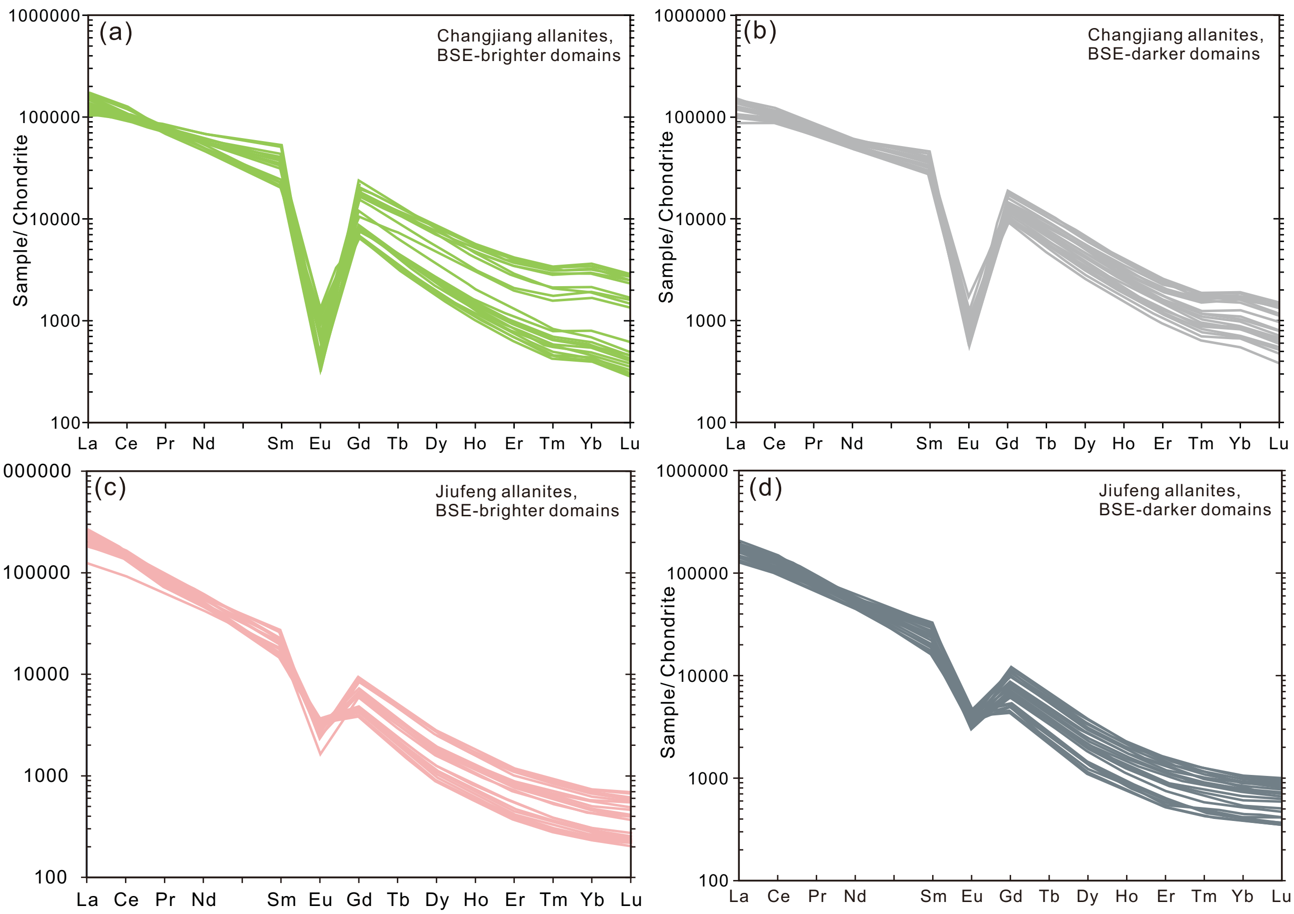
(a)
Changjiang allanites,
BSE-brighter domains
Sample/ Chondrite
1000000
100000
10000
1000
100
La Ce Pr Nd Sm Eu Gd Tb Dy Ho Er Tm Yb Lu
(b)
Changjiang allanites,
BSE-darker domains
(c)
Jiufeng allanites,
BSE-brighter domains
(d)
Jiufeng allanites,
BSE-darker domains

DOI: https://doi.org/10.2138/am-2022-8531. http://www.minsocam.org/

Figure 11

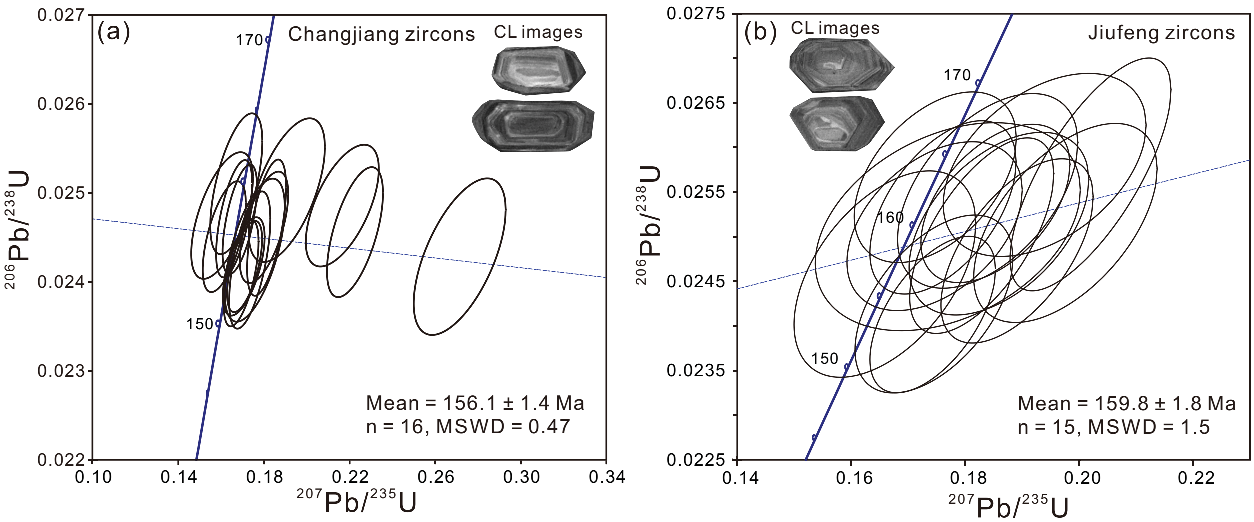

This is the peer-reviewed, final accepted version for American Mineralogist, published by the Mineralogical Society of America.
The published version is subject to change. Cite as Authors (Year) Title. American Mineralogist, in press.
DOI: https://doi.org/10.2138/am-2022-8531. http://www.minsocam.org/

Figure 12

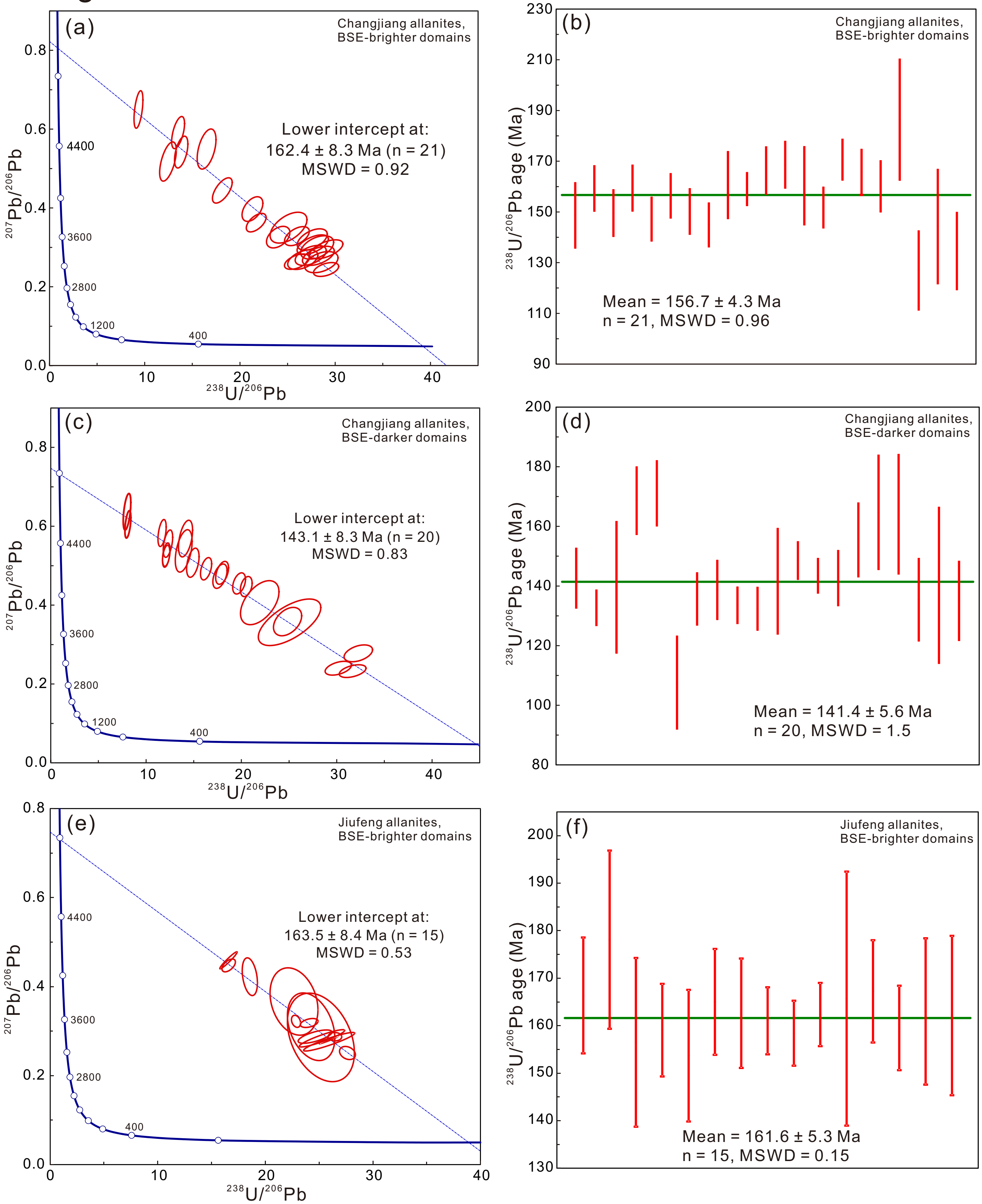

Figure 13

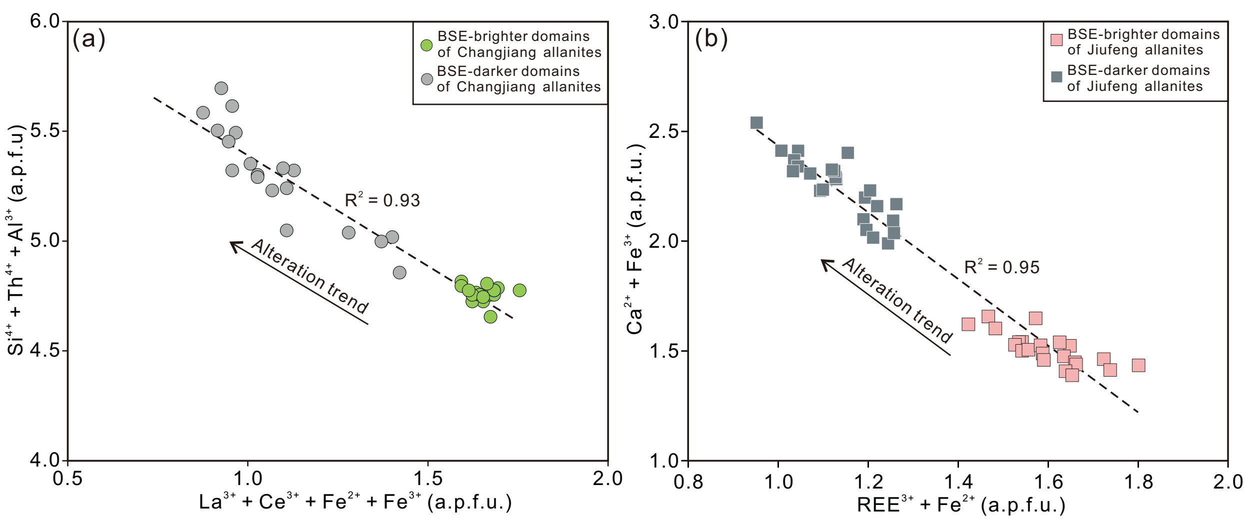
(a)
BSE-brighter domains of Changjiang allanites
BSE-darker domains of Changjiang allanites
R² = 0.93
Alteration trend
Si⁴⁺ + Th⁴⁺ + Al³⁺ (a.p.f.u)
La³⁺ + Ce³⁺ + Fe²⁺ + Fe³⁺ (a.p.f.u.)
6.0
5.5
5.0
4.5
4.0
0.5
1.0
1.5
2.0
(b)
BSE-brighter domains of Jiufeng allanites
BSE-darker domains of Jiufeng allanites
R² = 0.95
Alteration trend
Ca²⁺ + Fe³⁺ (a.p.f.u.)
REE³⁺ + Fe²⁺ (a.p.f.u.)
3.0
2.5
2.0
1.5
1.0
0.8
1.0
1.2
1.4
1.6
1.8
2.0

Figure 14

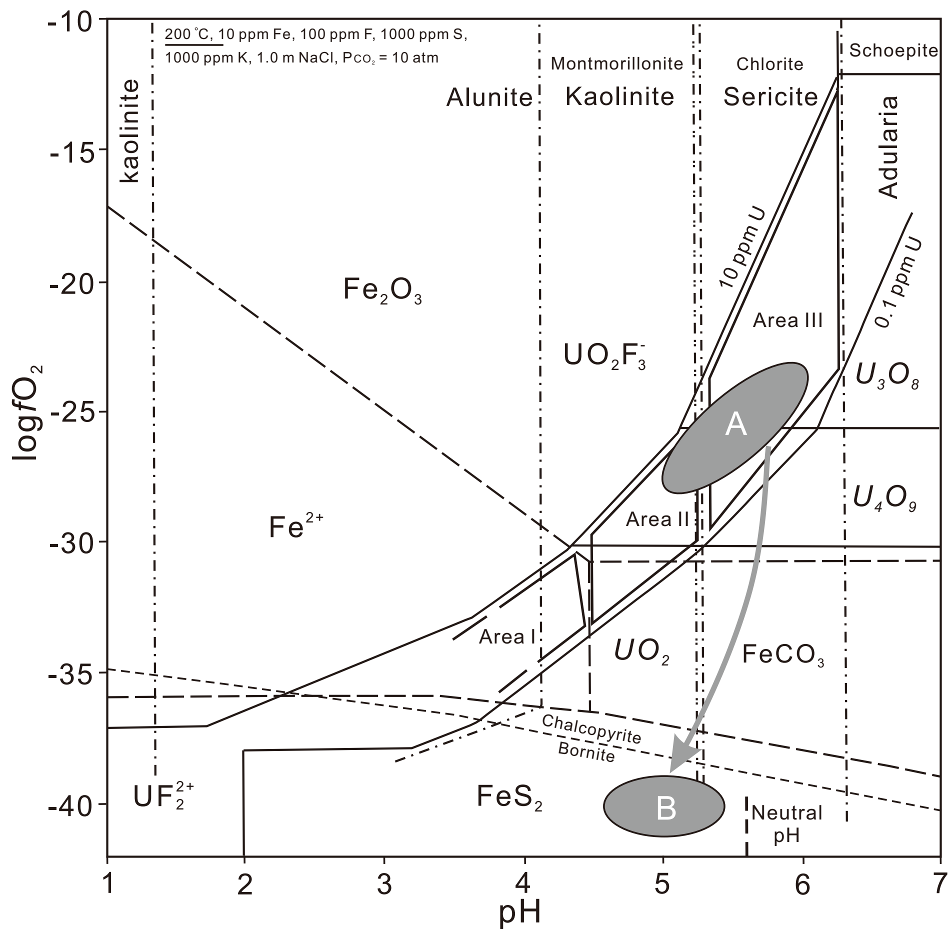
200 °C, 10 ppm Fe, 100 ppm F, 1000 ppm S,
1000 ppm K, 1.0 m NaCl, PCO2 = 10 atm
kaolinite
Alunite
Montmorillonite
Kaolinite
Chlorite
Sericite
Schoepite
Adularia
10 ppm U
0.1 ppm U
Fe2O3
UO2F3-
Area III
U3O8
A
U4O9
Fe2+
Area II
Area I
UO2
FeCO3
Chalcopyrite
Bornite
UF2 2+
FeS2
B
Neutral pH
logfO2
pH
-10
-15
-20
-25
-30
-35
-40
1
2
3
4
5
6
7